



Northwest Africa 773: Lunar origin and iron-enrichment trend

T. J. FAGAN,^{1†*} G. J. TAYLOR,¹ K. KEIL,¹ T. L. HICKS,¹ M. KILLGORE,² T. E. BUNCH,³
J. H. WITTKE,⁴ D. W. MITTFELDLT,⁵ R. N. CLAYTON,⁶ T. K. MAYEDA,⁶ O. EUGSTER,⁷
S. LORENZETTI,⁷ and M. D. NORMAN⁸

¹Hawai'i Institute of Geophysics and Planetology, School of Ocean and Earth Science and Technology,
University of Hawai'i at Manoa, Honolulu, Hawai'i 96822, USA

²P.O. Box 95, Southwest Meteorite Lab, Payson, Arizona 85547, USA

³Space Sciences Division, NASA Ames Research Center, Moffett Field, California 94035, USA

⁴Department of Geology, Northern Arizona University, Flagstaff, Arizona 86011, USA

⁵NASA Johnson Space Center, Houston, Texas 77258, USA

⁶Enrico Fermi Institute, University of Chicago, Chicago, Illinois 60637, USA

⁷Physikalisches Institut, University of Bern, 3012 Bern, Switzerland

⁸Research School of Earth Sciences, Australian National University, Canberra 0200 ACT, Australia

†Present address: Tokyo Institute of Technology, 2–12–1 Ookayama, Meguroku, Tokyo 152–8551, Japan

*Corresponding author. E-mail: fagan@geo.titech.ac.jp

(Received 19 August 2002; revision accepted 9 October 2002)

Abstract—The meteorite Northwest Africa 773 (NWA 773) is a lunar sample with implications for the evolution of mafic magmas on the moon. A combination of key parameters including whole-rock oxygen isotopic composition, Fe/Mn ratios in mafic silicates, noble gas concentrations, a KREEP-like rare earth element pattern, and the presence of regolith agglutinate fragments indicate a lunar origin for NWA 773. Partial maskelynitization of feldspar and occasional twinning of pyroxene are attributed to shock deformation. Terrestrial weathering has caused fracturing and precipitation of Ca-rich carbonates and sulfates in the fractures, but lunar minerals appear fresh and unoxidized.

The meteorite is composed of two distinct lithologies: a two-pyroxene olivine gabbro with cumulate texture, and a polymict, fragmental regolith breccia. The olivine gabbro is dominated by cumulate olivine with pigeonite, augite, and interstitial plagioclase feldspar. The breccia consists of several types of clasts but is dominated by clasts from the gabbro and more FeO-rich derivatives. Variations in clast mineral assemblage and pyroxene Mg/(Mg + Fe) and Ti/(Ti + Cr) record an igneous Fe-enrichment trend that culminated in crystallization of fayalite + silica + hedenbergite-bearing symplectites.

The Fe-enrichment trend and cumulate textures observed in NWA 773 are similar to features of terrestrial ponded lava flows and shallow-level mafic intrusives, indicating that NWA 773 may be from a layered mafic intrusion or a thick, differentiated lava flow. NWA 773 and several other mafic lunar meteorites have LREE-enriched patterns distinct from Apollo and Luna mare basalts, which tend to be LREE-depleted. This is somewhat surprising in light of remote sensing data that indicates that the Apollo and Luna missions sampled a portion of the moon that was enriched in incompatible heat-producing elements.

INTRODUCTION

Igneous rocks from the moon provide invaluable sources of information regarding planetary scale differentiation of the moon (Warren 1985; Schmitt 1991; Hess and Parmentier 1995; Shearer and Papike 1999) and melting and differentiation processes that affected specific lunar rock suites (Neal and Taylor 1992; Neal et al. 1994; Ryder and

Schuraytz 2001). Most of the available lunar igneous rocks come from the Apollo and Luna missions (Warren 1993). Lunar meteorites comprise a much smaller data set than the Apollo and Luna samples, but the meteorites offset key limitations of the return mission samples. The Apollo and Luna missions are from a limited portion of the moon concentrated on the lunar maria (Warren and Kallemeyn 1991a). The mare basalts from these regions compose nearly

one-fifth of the lunar near-side surface, but only about 1% of the lunar crust (Head and Wilson 1992). Furthermore, remote sensing studies show that the Apollo and Luna missions sampled a portion of the moon anomalously enriched in incompatible heat-producing elements (Jolliff et al. 2000; Lawrence et al. 2000). The geochemically anomalous and spatially restricted nature of the areas sampled during the Apollo and Luna missions results in a sample set that, although extraordinarily valuable, cannot be considered representative of the lunar crust.

In light of these limitations, lunar meteorites provide an important complement to the Apollo and Luna samples. Obviously, interpretation of the lunar meteorites is hindered because we cannot specify a priori the precise location on the moon from which a given meteorite originates. Lunar meteorites may come from anywhere on the moon, and thus, are not necessarily restricted to a limited region of the near-side. With continuing exploration of Antarctica and hot deserts, the number of identified lunar meteorites is increasing to the point where geochemical patterns characteristic of meteorites can be discussed and compared with systematics of the Apollo and Luna samples (Snyder et al. 1999a; Warren and Kallemeyn 1991b; Arai et al. 2002).

In this paper, we describe the lunar meteorite, Northwest Africa (NWA) 773, document its lunar origin, discuss its implications for petrogenesis of lunar mafic rocks, and compare this meteorite with geochemical patterns associated with specific stages of magmatic evolution of the moon (Shearer and Papike 1999). The meteorite consists of two texturally distinct lithologies: a dark gray, fragmental, regolith breccia; and a green, two-pyroxene, olivine gabbro (Fig. 1). We argue that the olivine gabbro and clasts in the breccia record a complex igneous differentiation history. The geochemistry of NWA 773 is similar in some respects to other mafic lunar meteorites but distinct from typical Apollo and Luna mare basalts (Snyder et al. 1999b; Shearer and Papike 1999).

ANALYTICAL METHODS

Petrography and Mineral Compositions

Three polished thin sections of NWA 773 were examined using petrographic microscopes. Backscattered electron (BSE) images, elemental X-ray maps, and quantitative analyses of phases were collected using a Cameca SX-50 electron microprobe at the University of Hawai'i and a Cameca MBX electron microprobe at Northern Arizona University. Two large-scale elemental maps of Na, Mg, Al, Si, P, K, Ca, Ti, Cr, and Fe K α were collected using a 15 keV, 50 nA focused electron beam, with step sizes of 9 μ m for one thin section and 18 μ m for the other section. The elemental maps were combined using image processing software and were used to estimate mineral modes (Hicks et al. 2000, 2002). Modal estimates were based on 1.3×10^5 counts from

approximately 81 mm² from one thin section of the breccia and 4.3×10^5 counts from 104 mm² from two thin sections of the olivine gabbro. Modes and mean mineral compositions (determined by electron microprobe analyses; see below) were combined to provide an estimate of major elemental composition of the olivine gabbro. Compositions of minerals in the polymict breccia portion of NWA 773 vary over wide ranges in different types of clasts; thus, the elemental composition of the breccia was not estimated by modal recombination.

Quantitative mineral compositions were determined using wavelength dispersive analyses based on well-characterized oxide and silicate standards. A 15 keV voltage and peak and background counting times of 12 to 30 s were used for all analyses, but current and spot size varied depending on the phase analyzed and the goal of the specific analyses. Most silicates and oxides were analyzed using a focused beam (~1 μ m diameter) and 20 nA current. The current was lowered to 10 nA for many feldspar and Ca-phosphate analyses. A 10 nA beam rastering over an area of approximately 12 \times 8 μ m was used for analyses of glass in melt inclusions, a glass spherule, and a fragment of regolith agglutinate. We normalized oxide and silicate mineral formulae assuming that Ti and Cr are present as Ti⁴⁺ and Cr³⁺, though we recognize that some Ti³⁺ and Cr²⁺ may be present.

Bulk Elemental Composition

We initially obtained a small, ~200 mg chip of NWA 773 dominated by the breccia lithology with a small green clast similar to the olivine gabbro for whole-rock geochemical analysis. We prepared two samples for geochemical analysis from this chip. We separated an ~14 mg sample of pure olivine-gabbro-like material, which we refer to as "clast," and then ground and homogenized the remaining material as a breccia lithology sample. An ~23 mg split of the breccia lithology was taken for instrumental neutron activation analysis (INAA). Subsequent to INAA on these samples, we received a second, ~325 mg chip of the olivine gabbro. This sample was ground and homogenized, and an ~39 mg split was taken for INAA. An ~20 mg split of the homogenized powder of the breccia was fused into a glass bead in an Ar atmosphere, following Brown (1977), for major element analysis via electron microprobe (FB-EMPA). A split of the olivine gabbro lithology failed to form a homogeneous glass bead—quench crystals of olivine were ubiquitous on the surface of the bead. Analyses of the fused beads were done on the JSC SX100 probe. Analytical conditions were 15 kV and 15 nA, with a focused beam rastered over a 10 \times 10 μ m area.

Samples, standards, and controls were sealed in pure silica glass tubes for INAA. The INAA was done in two irradiations using standard JSC procedures (Mittlefehldt 1994). The breccia lithology and the clast sample were irradiated at a flux of 5.5×10^{13} n cm⁻² s⁻¹ for 20 hr. The

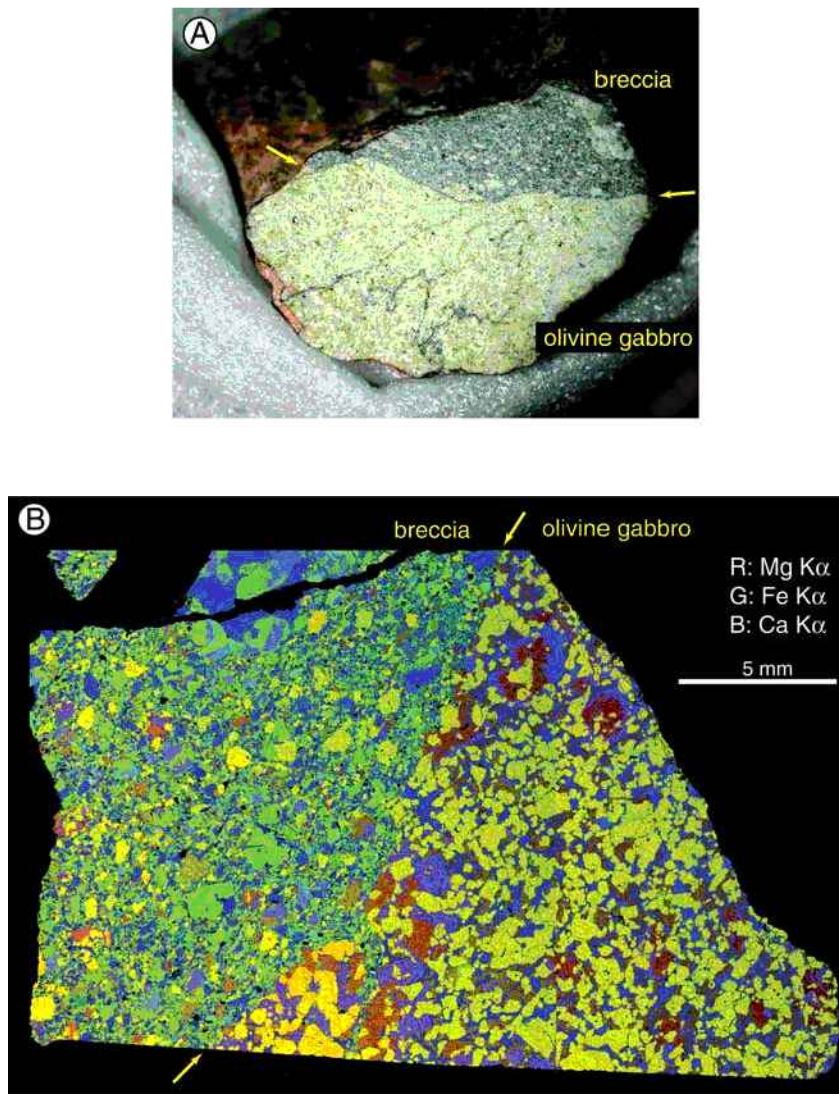


Fig. 1. a) Photograph of a cut surface of Northwest Africa 773, and b) elemental X-ray map of a thin section, with red = Mg $K\alpha$; green = Fe $K\alpha$; and blue = Ca $K\alpha$. Both images show a sharp boundary dividing breccia matrix (dark gray in [a], Fe-rich composition evident in [b]) from the olivine gabbro lithology. The olivine gabbro is considered a large lithic fragment in the breccia. In the elemental map (b), minerals in the olivine gabbro lithology consist of olivine (yellow), pigeonite (orange), augite (purple), and feldspars (blue), with minor Fe-oxide, sulfide, and metal (green). Minor compositions vary more widely in the breccia, but the following generalizations hold for the breccia portion of (b): blue = feldspars; yellow to yellow-orange = olivine; orange = pigeonite; green = fayalite or hedenbergite; purple = augite; black (rare) = silica.

samples were counted 4 times at roughly 0.5, 1, 4, and 8 weeks after irradiation to obtain data for nuclides of differing half-lives. The olivine gabbro lithology sample was irradiated at a flux of $5.5 \times 10^{13} \text{ n cm}^{-2} \text{ s}^{-1}$ for 16 hr and counted 3 times at roughly 0.5, 1, and 4 weeks after irradiation.

Splits from the “clast” and breccia powders were also analyzed by inductively-coupled plasma mass spectroscopy (ICP-MS). These analyses were completed after the manuscript was submitted for review and the data are presented in the Appendix. The ICP-MS results are consistent with the INAA data, which were submitted with the original manuscript for review. The ICP-MS data were obtained by

solution aspiration of the dissolved sample into an Agilent 7500 quadrupole ICP-MS using a quartz concentric nebulizer and a double pass spray chamber, following procedures described by Norman et al. (1998) and Norman and Mittlefehldt (2002). Solutions were prepared by dissolving 50 mg of sample in HF-HCl-HNO₃. The sample was converted to nitrates and brought up in 50 ml of 5% HNO₃ for analysis. Distilled reagents were used throughout. Beryllium (50 ppb), As (10 ppb), In, Re, and Bi (5 ppb) were added to each solution as internal standards. The analyses were calibrated against BHVO-1, with USGS reference materials W-2, BIR-1, BCR-2, and AGV-1 used for quality control.

Bulk Oxygen Isotopes and Noble Gases

A chip and a few fragments of breccia and olivine gabbro were plucked from a sawed slab with no visible fusion crust and were prepared for oxygen isotopic and noble gas analyses. The oxygen isotopic compositions of the two lithologies of NWA 773 were determined using the methods of Clayton and Mayeda (1963, 1983). The noble gas isotopic abundances were determined from a sample of the olivine gabbro lithology of 18.4 mg and a sample of the cataclastic breccia fraction of ~46 mg. The breccia sample was crushed in a stainless steel mortar and separated into 3 grain-size fractions by sieving in acetone: 340–750 μm (15.84 mg), 35–340 μm (15.01 mg), and <35 μm (14.65 mg). The purpose of this separation was to check for enrichment of the surface-correlated trapped solar gases relative to the volume-correlated cosmic ray-produced and radiogenic gases. The samples were heated in vacuum at 90°C for several days in the extraction system to remove adsorbed atmospheric gases. He, Ne, and Ar were extracted by radiofrequency heating in a single step at 1700°C and then analyzed in the mass spectrometer system B at the University of Bern. All details concerning the instrument, analytical procedure, background, and blank corrections have been described in detail previously (Eugster et al. 1993).

MINERALOGY AND TEXTURES

The meteorite consists of three stones that were purchased from nomads near Dchira, Western Sahara in September 2000. The nomads brought one of us (M. Killgore) to the find site and showed the find location of each stone

within an area less than 5 m². Prior to breakage into splits for analyses, the three stones had masses of 359 g, 224 g, and 50 g and had interlocking surfaces suggesting that they were broken from a common precursor. The 2 larger stones consist of subequal proportions of dark gray fragmental breccia and green olivine gabbro. The smallest stone consists predominantly of the olivine gabbro lithology. Of the 3 thin sections examined during this study, 2 come from the largest stone, and one is from the smallest. No fusion crust was identified in thin section, but a very thin crust appears to be present in places. The external surface of the meteorite is brown on the breccia lithology and black on the olivine gabbro lithology.

The sharp boundary between the olivine gabbro and breccia lithologies is apparent both on a fresh surface and from a thin-section-scale elemental map (Fig. 1), which reflects the higher olivine abundance and Mg/(Mg + Fe) of the olivine gabbro (Tables 1, 2, and 3). No chilled margin or baked zone is observed along the contact between the olivine gabbro and the breccia. In the hand sample, green gabbroic fragments similar to the olivine gabbro lithology occur as clasts ranging up to several cm across in the breccia. Boundaries between these clasts and breccia matrix appear to be identical to the boundary between the olivine gabbro and the matrix. Thus, the olivine gabbro was, likely, simply a large clast in the breccia, and NWA 773 was broken along the interior of the clast.

Terrestrial weathering has resulted in the fracturing of most grains larger than about 100 μm across (Fig. 2), and many of the fractures are filled with Ca-carbonates and sulfates. Except for fracturing and precipitation in the fractures, lunar minerals in the meteorite show minimal alteration: no hydrous

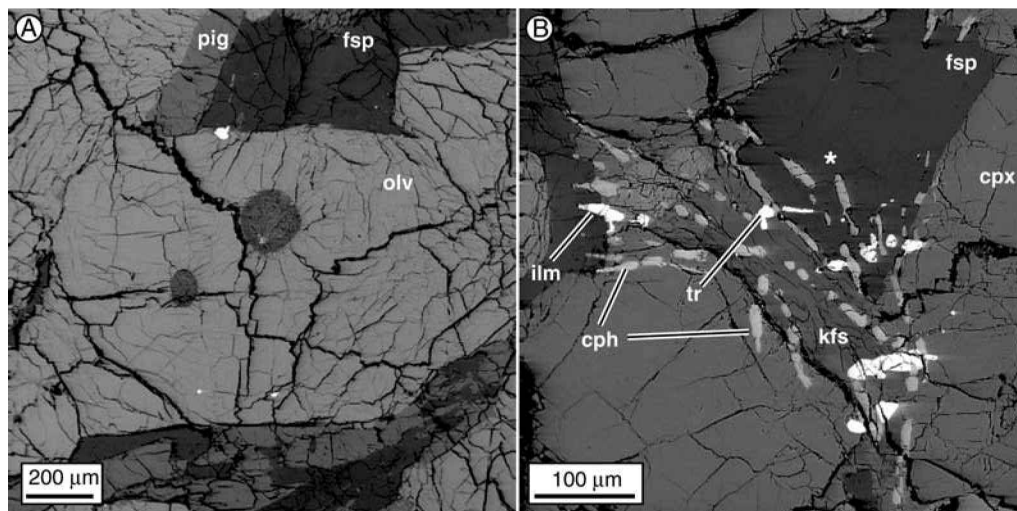


Fig. 2. Backscattered electron images of the NWA 773 olivine gabbro lithology: a) large cumulate olivine (olv) with adjacent pigeonite (pig) and plagioclase feldspar (fsp). The BSE-bright grain along the boundary of olivine and feldspar is Cr-spinel. Two rounded pyroxene-phyric melt inclusions are trapped within the large olivine grain. The weathering veins are black in this image and are dominated by voids and Ca-rich carbonate; b) residual pocket of phases enriched in incompatible elements. Mineral abbreviations: kfs = K, Ba-feldspar; cph = Ca-phosphates; ilm = ilmenite; tr = troilite; fsp = plagioclase feldspar; cpx = augite. The asterisk marks the location of the An-poor analysis (An₇₅) in Table 5.

alteration of lunar minerals was observed; metal, troilite, and Fe, Ti-oxides appear free of rust in the thin section; unfractured grain boundaries appear sharp and free of hydrous alteration or rust; the rock is well-indurated.

Olivine Gabbro Lithology

The olivine gabbro appears light green on a fresh surface because of the abundance of coarse-grained olivine and pyroxenes (Fig. 1). Our modal estimate (Table 1) indicates that this portion of NWA 773 should be classified as a two-pyroxene olivine gabbro. A more olivine-rich composition from another specimen of NWA 773 has been classified as feldspathic lherzolite (Bridges et al. 2002).

Olivine crystals are equant to slightly elongate, euhedral to subhedral grains forming a loose aggregate characteristic of cumulate rocks. Olivine occupies approximately 55 vol% of this lithology (Table 1) and individual crystals range up to 1300 μm across in the thin section (Fig. 2a). Undulatory extinction is characteristic, indicating deformation of the crystal lattice. Olivine compositions in the olivine gabbro vary over a limited range near Fo_{68} (Table 2; Fig. 3). All of the 120 analyses collected at the University of Hawai'i in this lithology yield compositions ranging between Fo_{66} and Fo_{72} , with a mean of Fo_{68} . The individual olivine crystals appear to be unzoned. The ratios of Fe/Mn are comparable to lunar olivines (Fig. 3).

Two types of melt inclusions are trapped within the olivine crystals. One type is characterized by fine-grained dendritic pyroxene in a glass matrix (Fig. 2a) and is broadly andesitic in composition, with a mean SiO_2 concentration of 61 wt% (Table 3). In some cases, branches of dendritic pyroxene appear to radiate from common nucleation points in the melt inclusions. The other type of melt inclusion is much more silicic (Table 3) and is devoid of dendritic pyroxene. These silica-rich inclusions are generally aphyric, but in some cases, 1 or 2 Ca-phosphate crystals may be present. Multiple melt inclusions of the same type are found in the same crystal (Fig. 2a), but both types of inclusions have not been identified together in a single olivine host.

Olivine crystals in the olivine gabbro are in contact with, and in some cases, rimmed by subhedral pigeonite. Pigeonite, in turn, occurs in contact with and may be rimmed by augite.

Table 1. Modal abundances of NWA 773.

	Olivine gabbro	Breccia
Olivine	55.5	21
Pigeonite	18.9	39
Augite	8.7	17
Plagioclase	14.2	19
K, Ba feldspar	1.6	2.5
Chromite	0.9	0.3
Fe, Ti oxides	0.3	0.1
Silica	0	0.8
Ca phosphate	<0.2	0.2

Table 2. Representative electron microprobe analyses (wt%) of olivines from NWA 773.

Clast type (breccia)	Olivine Gabbro	Breccia		
		Gabbro	Fe-rich lithic	Symplectite
SiO_2	37.2	35.9	29.2	29.6
TiO_2	<0.03	0.06	0.13	0.12
Al_2O_3	<0.02	0.03	<0.02	<0.02
Cr_2O_3	0.07	0.09	0.05	<0.04
FeO	28.5	33.6	68.3	64.4
MnO	0.27	0.29	0.76	0.63
MgO	33.8	29.9	0.94	4.23
CaO	0.24	0.34	0.46	0.31
Total	100.2	100.1	99.8	99.4
Structural formulae based on 4O				
Si	0.996	0.988	0.987	0.984
Ti	b.d. ^a	0.001	0.003	0.003
Al	b.d.	0.001	b.d.	b.d.
Cr	0.001	0.002	0.001	b.d.
Fe	0.639	0.774	1.93	1.79
Mn	0.006	0.007	0.022	0.018
Mg	1.35	1.23	0.047	0.209
Ca	0.007	0.010	0.017	0.011
Total	3.00	3.01	3.01	3.01
Fo	68	61	2	10

^ab.d. = below detection.

Pigeonite is more abundant (Table 1) and tends to be coarser-grained than augite, but both types of pyroxene range up to 1000 μm across. Pyroxene crystals are equant with anhedral to subhedral form. No exsolution lamellae were identified in our samples at the spatial resolution of SEM and EPMA observations. However, 1- μm -scale lamellae in another specimen of NWA 773 have been reported by Korotev et al. (2002). Twin lamellae were identified in some of the pigeonite, and all of the pyroxene exhibits undulatory extinction, indicating that NWA 773 was deformed after crystallization. Pyroxenes in the olivine gabbro have limited compositional ranges near $\text{Wo}_{11}\text{En}_{65}$ and $\text{Wo}_{36}\text{En}_{50}$ and are separated by a well-defined compositional gap (Table 4; Fig. 4). Mineral normalizations of EPMA data suggest that all the Fe is ferrous, unlike pyroxene from terrestrial mafic rocks. Ratios of Fe/Mn in the pyroxene from the olivine gabbro are consistent with a lunar or terrestrial origin (Fig. 3), but the apparent absence of ferric iron indicates a non-terrestrial origin.

Aluminum, Ti, and Cr occur in the pyroxenes in minor concentrations (Table 4). Most analyses of pyroxene from the olivine gabbro have $\text{Ti}/\text{Al} = 0.25$ and all results yield $\text{Ti}/\text{Al} < 0.5$ (Fig. 5). Analyses with relatively high Ti/Al also tend to have high $\text{Ti}/(\text{Ti} + \text{Cr})$, consistent with late-stage crystallization in a system that fractionated compatible Cr and incompatible Ti. Higher $\text{Ti}/(\text{Ti} + \text{Cr})$ in pyroxene correlates with more Fe-rich compositions, but the variation in Fe

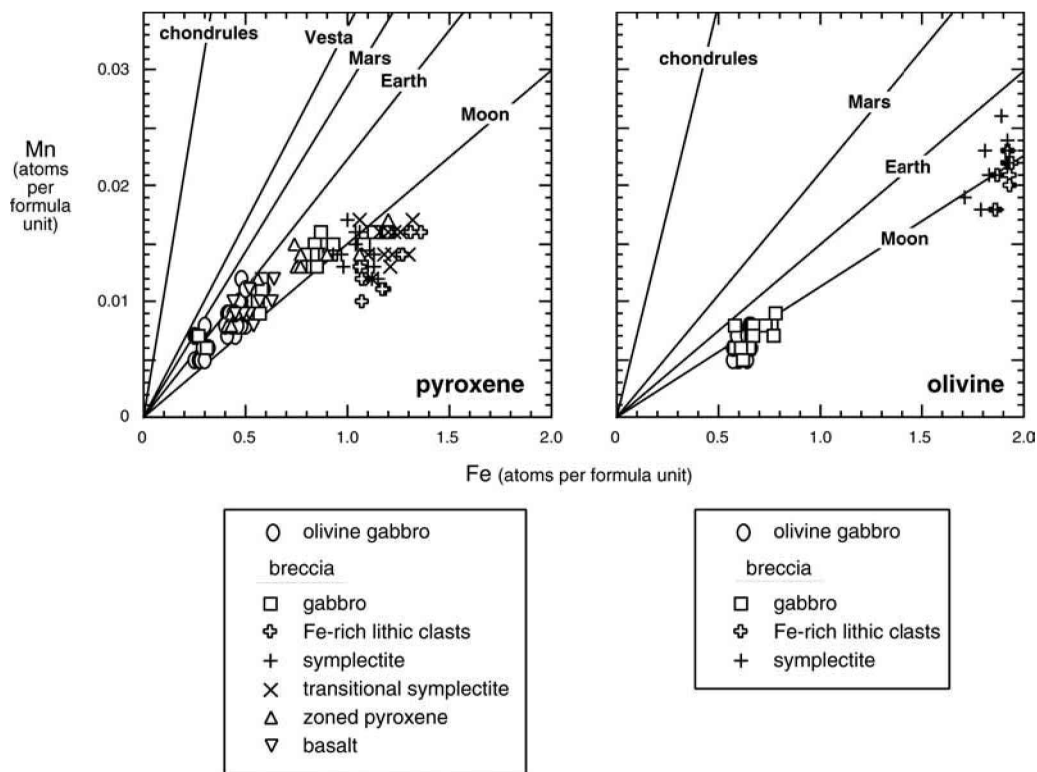


Fig. 3. Concentrations of Fe and Mn in olivine and pyroxene from NWA 773. The atoms per formula unit is based on 4 oxygen for olivine and 6 oxygen for pyroxene. The ratios of Fe/Mn associated with specific parent bodies are from Papike (1998).

Table 3. Mean ($\pm 1\sigma$, and *minimum – maximum*) results of analyses of glassy phases in Northwest Africa 773.

	Yellow-green spherule n = 22	Agglutinate glass n = 12	Pyroxene phyric melt inclusions in olivine n = 66	Aphyric melt inclusions in olivine n = 16
SiO ₂	43.3 \pm 0.3 42.7 – 43.8	44.0 \pm 0.2 43.6 – 44.5	61.2 \pm 3.8 54.8 – 69.9	79.1 \pm 5.1 70.8 – 87.0
TiO ₂	1.42 \pm 0.05 1.33 – 1.52	0.19 \pm 0.07 0.10 – 0.35	2.2 \pm 0.5 1.2 – 3.2	0.39 \pm 0.25 0.22 – 1.29
Al ₂ O ₃	15.0 \pm 0.1 14.8 – 15.2	32.4 \pm 0.5 31.3 – 33.0	14.3 \pm 0.8 12.4 – 16.1	8.9 \pm 2.0 5.8 – 12.3
Cr ₂ O ₃	0.29 \pm 0.04 0.21 – 0.37	<0.07 <0.07 – 0.10	<0.07 <0.07 – 0.18	<0.07 <0.07 – 0.08
FeO	15.6 \pm 0.3 15.2 – 16.4	2.8 \pm 0.4 2.1 – 3.4	4.5 \pm 1.7 1.3 – 7.8	1.5 \pm 1.4 0.8 – 6.6
MnO	0.22 \pm 0.03 0.16 – 0.28	<0.06 <0.06 – 0.08	0.07 \pm 0.04 <0.06 – 0.14	<0.06 <0.06 – 0.07
MgO	11.1 \pm 0.1 10.9 – 11.3	2.08 \pm 0.15 1.86 – 2.35	2.0 \pm 0.6 0.6 – 3.6	0.57 \pm 1.51 <0.02 – 6.2
CaO	11.6 \pm 0.1 11.3 – 11.7	17.8 \pm 0.3 17.1 – 18.1	13.2 \pm 1.8 8.9 – 16.0	3.2 \pm 2.7 1.1 – 10.2
Na ₂ O	0.03 \pm 0.01 <0.03 – 0.06	0.36 \pm 0.03 0.32 – 0.41	0.77 \pm 0.26 0.37 – 1.77	1.0 \pm 0.7 0.4 – 2.4
K ₂ O	<0.03 <0.03 – 0.04	0.03 \pm 0.02 <0.03 – 0.06	0.16 \pm 0.07 0.04 – 0.43	3.1 \pm 2.4 0.4 – 7.1
P ₂ O ₅	<0.06 <0.06 – 0.07	<0.06 <0.06 – 0.08	0.34 \pm 0.10 0.14 – 0.60	<0.06 <0.06 – 3.4
Total	98.6 \pm 0.5 97.8 – 99.6	99.7 \pm 0.3 99.0 – 100.1	98.8 \pm 0.5 97.3 – 99.8	98.2 \pm 0.6 97.3 – 99.3

Table 4. Representative electron microprobe analyses (wt%) of pyroxenes from NWA 773.

Pyroxene clast type (breccia)	Olivine gabbro		Breccia								
	Pigeonite	Augite	Pigeonite single mineral	Pig-Aug ^a single mineral	Augite gabbro	Hedenbergite fayalite gabbro	Hedenbergite symplectite	Pigeonite zoned pyx.	Augite zoned pyx.	Pigeonite basalt	Augite basalt
SiO ₂	52.8	52.4	53.0	49.9	51.8	46.0	45.1	50.0	50.3	51.8	48.6
TiO ₂	0.40	0.22	0.15	0.34	0.31	1.03	1.37	0.37	0.39	0.67	1.46
Al ₂ O ₃	1.50	1.68	0.98	1.14	2.41	1.08	1.43	1.32	2.20	1.85	3.97
Cr ₂ O ₃	0.62	0.77	0.55	0.25	1.08	0.06	<0.04	0.59	1.04	1.24	1.61
FeO	15.6	8.40	19.0	25.5	8.75	30.5	31.96	23.87	13.6	17.46	14.2
MnO	0.25	0.22	0.34	0.38	0.23	0.33	0.37	0.42	0.27	0.25	0.28
MgO	23.3	17.9	22.5	13.1	17.8	1.58	1.24	14.7	15.1	22.3	15.1
CaO	5.60	17.5	3.23	8.86	17.0	18.1	16.8	8.50	16.3	3.83	13.9
Na ₂ O	<0.02	0.04	<0.02	<0.02	0.03	0.03	<0.02	<0.02	0.03	<0.02	<0.02
Total	100.1	99.1	99.7	99.5	99.4	99.3	98.4	99.7	99.2	99.4	99.1
Structural formulae based on 6O											
Si	1.94	1.94	1.97	1.95	1.92	1.93	1.91	1.94	1.91	1.92	1.85
ivAl	0.064	0.055	0.035	0.046	0.080	0.053	0.071	0.060	0.089	0.076	0.153
Total tet. ^b	2.00	2.00	2.00	2.00	2.00	1.98	1.98	2.00	2.00	2.00	2.00
Ti	0.011	0.006	0.004	0.010	0.009	0.033	0.044	0.011	0.011	0.019	0.042
viAl	0.065	0.074	0.043	0.053	0.105	0.053	0.071	0.060	0.098	0.081	0.178
Cr	0.018	0.022	0.016	0.008	0.032	0.002	b.d. ^c	0.018	0.031	0.036	0.048
Fe	0.477	0.261	0.589	0.834	0.271	1.068	1.131	0.773	0.430	0.542	0.450
Mn	0.008	0.007	0.011	0.013	0.007	0.012	0.013	0.014	0.009	0.008	0.009
Mg	1.275	0.990	1.244	0.764	0.983	0.099	0.078	0.847	0.855	1.236	0.857
Ca	0.220	0.696	0.129	0.371	0.675	0.811	0.762	0.353	0.664	0.153	0.567
Na	b.d.	0.003	b.d.	b.d.	0.002	b.d.	b.d.	b.d.	0.002	b.d.	b.d.
Total	4.01	4.00	4.00	4.01	4.00	4.01	4.01	4.01	4.01	4.00	4.00
Wo	11	36	7	19	35	41	39	18	34	8	30
En	65	51	63	39	51	5	4	43	44	64	46

^a“Pig-Aug” refers to pyroxenes with Wo₂₀.

^bTotal tet. = total of tetrahedral cations.

^cb.d. = below detection.

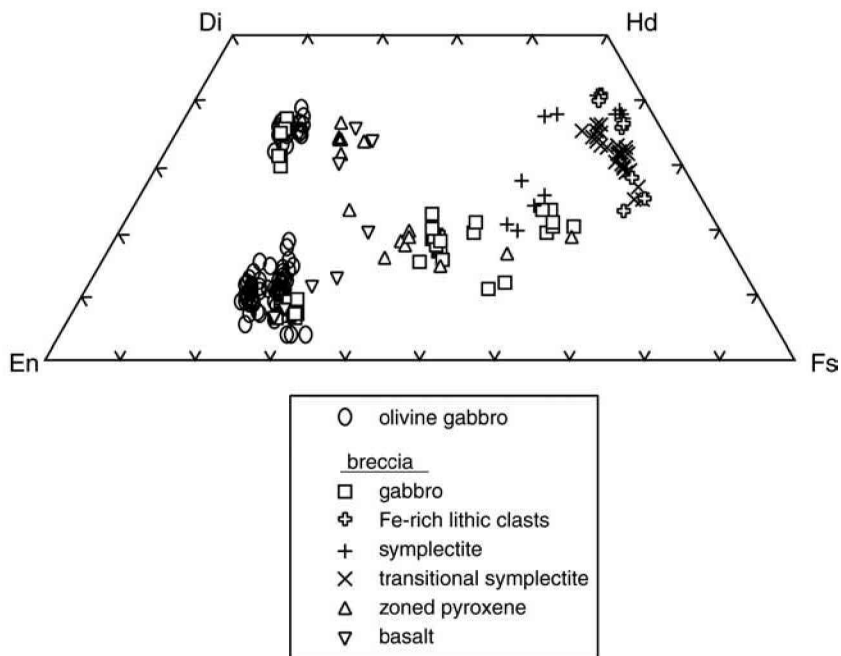


Fig. 4. Quadrilateral compositions of pyroxenes from NWA 773. Note the well-defined separation of low- and high-Ca pyroxenes in the olivine gabbro lithology.

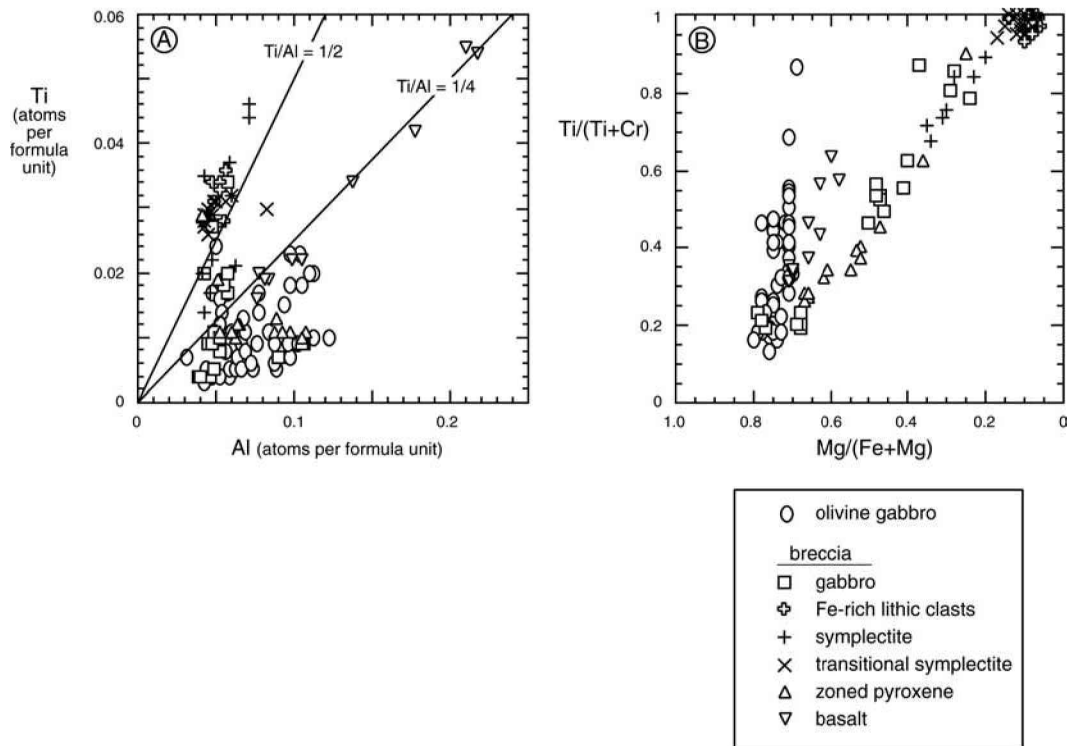


Fig. 5. Main “off-quadrilateral” components of pyroxenes from NWA 773: a) Ti versus Al in atoms per 6 oxygen formula unit; b) Ti# versus Mg#, with Mg# reversed so that crystal fractionation drives compositions away from the origin on both axes (see Arai et al. 1996). Note the Ti, Cr-rich compositions of pyroxene from the basaltic clast shown in Fig. 6d.

content is very slight, with $Mg/(Mg + Fe)$ from ~ 0.76 to 0.72 (see Fig. 5). The analysis with $Ti/(Ti + Cr) \sim 0.87$ is actually depleted in high field strength elements and constitutes a special case, as it is from a rare equant pyroxene trapped in a melt inclusion in olivine. The other analyses with high $Ti/(Ti + Cr)$ have relatively high Ti concentrations (>0.15 atoms per formula unit) and were determined in domains close to incompatible-element-rich residual melt pockets (see below).

Feldspars are anhedral, conforming to crystal margins of olivine and pyroxene, and occupy only 14 vol% of the olivine gabbro lithology in comparison to approximately 80 vol% mafic silicates (Table 1). In general, the feldspars are maskelynitized, but some feldspar domains exhibit birefringence. Plagioclase is, by far, the more abundant feldspar (Table 1) and occurs as relatively inclusion-free crystals up to several hundred μm across. In contrast, most alkali feldspar crystals are 50 to 100 μm across, with some crystals ranging up to 300 μm long, and are characterized by multiple inclusions of Ca-phosphates, ilmenite, and troilite (Fig. 2b). These minerals occur as inclusions entirely within alkali feldspar, along grain boundaries, and as inclusions clustered within 100 μm of alkali feldspar, but hosted in adjacent pyroxene or plagioclase (Fig. 2b).

Most analyses of plagioclase in the olivine gabbro lithology indicate compositions near $An_{90}Ab_{10}$ (Table 5). However, plagioclase in close proximity to alkali feldspar has

higher alkali contents (Table 5; An as low as An_{75} , Or as high as Or_{09}). Alkali feldspar is cathodoluminescent and is enriched in Ba as well as K (Table 5). During initial exposure to the electron beam, the K, Ba-feldspar luminesces a bright white or blue, and luminescence fades during exposure to the beam over the course of an analysis (1.5 min). Barium concentrations from 32 analyses of K, Ba-feldspar in the olivine gabbro range from 0.79–3.60 wt% BaO with a mean of 2.2 wt% (mean celsian content, Cs_{04}).

The K, Ba-feldspar crystals, together with associated splays of fine Ca-phosphates, ilmenite, and troilite, comprise incompatible-element-rich residual pockets enclosed within the framework of mafic silicates (Fig. 2b). Grains of Fe, Ni-metal also occur in the residual pockets but are rare. Ilmenite and Ca-phosphates occur as elongate prisms, typically on the order of 50 to 100 μm in length, while troilite grains tend to be equant and under 30 μm across. Significant MgO is present in the ilmenite (Table 6), similar to many lunar ilmenites. The Ca-phosphate prisms frequently consist of both apatite and whitlockite separated by a curved or irregular boundary. The high F contents of apatite (Table 7) are similar to apatites from the moon.

Chromian spinel occurs as equant, euhedral grains on the order of 100 μm across included in pyroxene and along pyroxene-olivine grain boundaries. In some cases, Cr-spinel conforms to the crystal outlines of adjacent olivine; rare Cr-

Table 5. Representative electron microprobe analyses (wt%) of feldspars and silica-rich glass from NWA 773.

Phase clast type (breccia)	Olivine gabbro			Breccia							
	Plagio- clase ^a	Plagio- clase ^b	K, Ba feldspar	Plagio- clase	Plagio- clase	K, Ba feldspar	Plagio- clase	Silica- rich glass	Silica- rich glass	Silica- rich glass	Silica- rich glass
				gabbro	gabbro	gabbro	symplec- tite	mineral	fayalite granite	symplec- tite	symplec- tite
SiO ₂	45.87	49.54	62.75	46.37	50.51	61.59	50.67	96.80	99.22	97.23	77.78
TiO ₂	<0.05	0.08	0.22	<0.05	<0.05	0.31	<0.05	0.33	0.25	0.17	0.12
Al ₂ O ₃	34.74	32.13	19.51	34.03	31.06	20.06	30.91	0.37	0.67	0.59	12.69
FeO	0.30	0.33	<0.07	0.49	0.88	0.33	1.11	0.75	0.15	1.09	1.08
MgO	0.17	0.17	<0.02	0.27	<0.02	<0.02	<0.02	<0.02	<0.02	<0.02	<0.02
CaO	17.95	15.00	0.40	17.97	14.41	0.89	14.01	0.05	<0.04	0.11	0.21
Na ₂ O	1.05	1.79	0.42	1.01	2.67	0.58	2.58	<0.04	0.18	<0.04	0.30
K ₂ O	0.14	1.38	15.10	0.11	0.51	14.19	0.58	0.22	0.24	0.14	4.59
BaO	n.a. ^c	0.13	1.97	<0.06	0.11	2.21	n.a.	n.a.	n.a.	n.a.	n.a.
Total	100.3	100.5	100.4	100.3	100.2	100.2	99.9	98.5	100.7	99.4	96.8
Structural formulae based on 8O (feldspars) and 2O (silica-rich glass)											
Si	2.11	2.26	2.93	2.13	2.31	2.88	2.32	0.990	0.998	0.987	0.852
Al	1.88	1.73	1.07	1.84	1.67	1.11	1.67	0.005	0.008	0.007	0.164
Total tet. ^d	3.99	3.99	3.99	3.97	3.98	3.99	3.99	0.99	1.00	0.99	1.02
Ti	b.d. ^e	0.003	0.008	b.d.	b.d.	0.011	b.d.	0.003	0.002	0.001	0.001
Fe	0.012	0.013	b.d.	0.019	0.034	0.013	0.043	0.006	0.001	0.009	0.010
Mg	0.012	0.012	b.d.	0.018	b.d.	b.d.	b.d.	b.d.	b.d.	b.d.	b.d.
Ca	0.884	0.734	0.020	0.885	0.705	0.045	0.687	0.001	b.d.	0.001	0.003
Na	0.094	0.159	0.038	0.090	0.237	0.053	0.229	b.d.	0.003	b.d.	0.006
K	0.009	0.080	0.898	0.007	0.030	0.848	0.034	0.003	0.003	0.002	0.064
Ba	n.a.	0.002	0.036	b.d.	0.002	0.041	n.a.	n.a.	n.a.	n.a.	n.a.
Total	5.00	4.99	5.00	4.99	4.99	5.00	4.98	1.01	1.01	1.01	1.10
An	90	75	2	90	73	5	72	–	–	–	–
Ab	10	16	4	9	24	5	24	–	–	–	–
Or	1	8	90	1	3	86	4	–	–	–	–
Cs	n.a.	0	4	0	0	4	n.a.	–	–	–	–

^aAnalysis from most common petrographic setting for plagioclase, interstitial to pyroxenes and olivines, and not in close proximity to K-feldspar.

^bAnalysis located in close proximity to adjacent K-feldspar crystal (150 μm, see Fig. 3b).

^cn.a. = not analyzed.

^dTotal tet. = Total tetrahedral cations.

^eb.d. = below detection.

spinel grains are included in olivine. The Cr-spinel is a solid solution with significant TiO₂ and MgO and yields stoichiometric compositions with all Fe assumed to be ferrous (Table 6).

Breccia Lithology

The breccia matrix appears dark gray to black on a fresh surface, but coarse clasts in the breccia exhibit a variety of shades of green and gray (Fig. 1). The breccia consists of a variety of types of fragments, many similar or plausibly linked to the adjacent olivine gabbro lithology. In spite of the similarities, modal abundances of the two lithologies clearly differ. The breccia has lower modal olivine and higher abundances of plagioclase feldspar and pyroxenes (Table 1; Fig. 1).

The breccia has a fragmental texture with a continuum in grain size from fine matrix grains (~5 μm) to coarse clasts (>1000 μm). Unlike many of the fragmental breccias collected during Apollo missions, the NWA 773 breccia is well-indurated and has minimal porosity. The breccia is

polymict, and the matrix appears to consist of fragments similar in lithology to the breccia clasts but broken into finer grain sizes. No whole-rock shock-melt glass was identified. However, mineral grains show clear signs of shock deformation, including maskelynitization of feldspar and undulatory extinction in olivine and pyroxene, similar to deformation of the olivine gabbro lithology. These observations are not repeated in the clast type descriptions that follow.

The description below is organized according to clast type. This description is representative, but not exhaustive, and focuses on the largest and most abundant clast types identified in the breccia.

Gabbro

Gabbroic clasts are characterized by coarse interlocking (“plutonic”) textures, plagioclase feldspar with compositions ranging between An₈₀ and An₉₆, and mafic silicates with Mg/(Mg + Fe) >0.2, but no higher than Mg/(Mg + Fe) values determined in the olivine gabbro lithology (Tables 2, 4, and 5). Most clasts that are considered “gabbroic” do not have the

Table 6. Representative electron microprobe analyses (wt%) of oxides from NWA 773.

Mineral clast type (breccia)	Olivine gabbro		Breccia	
	Cr-spinel	Ilmenite	Ulvö-spinel gabbro	Ilmenite gabbro
TiO ₂	11.8	55.7	29.9	52.4
Al ₂ O ₃	8.83	<0.02	2.60	0.03
Cr ₂ O ₃	34.7	0.58	6.27	0.30
FeO	38.6	38.8	59.8	45.9
MnO	0.30	0.37	0.28	0.31
MgO	4.32	5.25	0.58	0.65
CaO	0.06	<0.02	0.08	0.08
SiO ₂	0.15	0.18	0.19	0.11
Total	98.7	100.8	99.7	99.7
Structural formulae based on				
	4O	3O	4O	3O
Ti	0.311	1.002	0.828	0.992
Al	0.366	b.d. ^a	0.113	0.001
Cr	0.964	0.011	0.183	0.006
Fe	1.135	0.776	1.84	0.966
Mn	0.009	0.007	0.009	0.007
Mg	0.226	0.187	0.032	0.024
Ca	0.002	b.d.	0.003	0.002
Si	0.005	0.004	0.007	0.003
Total	3.02	1.99	3.02	2.00

^ab.d. = below detection.

full suite of major silicate minerals observed in the olivine gabbro lithology, namely olivine, pigeonite, augite, and plagioclase feldspar. However, many polymineralic gabbroic clasts have textures similar to those observed in the olivine gabbro: olivine appears to be rimmed by pigeonite; pigeonite and augite occur together along interlocking grain boundaries with no exsolution lamellae observed in pigeonite; spherical andesitic melt inclusions with dendritic pyroxene are present in some coarse olivine crystals; and interstitial K, Ba-feldspar crystals occur in some polycrystalline clasts. The grain sizes of the mafic silicates are comparable to those in the olivine gabbro, but do not range up to the coarsest sizes observed in the olivine gabbro lithology. Plagioclase feldspar grains in the gabbroic clasts are as coarse or coarser (up to ~1000 μm across; see Fig. 1) than their counterparts in the olivine gabbro lithology. Many coarse, single-mineral fragments are similar in composition, grain size, and grain shape to the polycrystalline gabbroic clasts and probably share a similar origin.

Olivine in gabbroic clasts in the breccia are broadly similar in composition to olivine from the olivine gabbro lithology but range to somewhat more Fe-rich compositions (minimum of Fo₅₅ compared to a minimum of Fo₆₆ in the olivine gabbro, see Fig. 3). In contrast, gabbroic pyroxene from the breccia exhibits a much wider range in composition than pyroxene from the olivine gabbro lithology. As is the case for olivine, some analyses of pyroxene from gabbroic

Table 7. Representative electron microprobe analyses (wt%) of Ca-phosphates from NWA 773.

Mineral clast type (breccia)	Olivine gabbro		Breccia	
	Whitlockite ^a	Apatite ^b	Apatite ^a symplectite	Apatite ^a symplectite
CaO	41.7	53.3	54.3	54.7
P ₂ O ₅	41.7	41.5	41.3	40.6
FeO	0.76	0.68	0.56	0.46
MgO	2.61	0.11	<0.02	<0.02
Na ₂ O	0.37	n.a. ^c	<0.03	<0.03
K ₂ O	0.05	n.a.	<0.03	<0.03
SiO ₂	0.84	0.54	0.33	0.39
Al ₂ O ₃	0.43	0.07	<0.03	<0.03
SrO	0.05	n.a.	0.08	0.10
La ₂ O ₃	0.84	n.a.	<0.05	<0.05
Ce ₂ O ₃	2.40	n.a.	0.03	0.2
SO ₃	0.05	n.a.	0.05	0.05
Cl	<0.04	0.16	0.13	0.2
F	3.75	3.82	3.60	3.75
Total	95.6	100.2	100.7	100.5
Nd ₂ O ₃ ^d	2.5	n.a.	n.a.	n.a.
Total	98.1	100.2	100.7	100.5
O == Cl, F	1.58	1.64	1.55	1.62
Total	96.5	98.6	99.1	98.8

Structural formulae based on

	8O	12.5O	12.5O	12.5O
Ca	2.49	4.86	4.95	5.02
P	1.97	2.99	2.97	2.94
Fe	0.035	0.048	0.040	0.033
Mg	0.217	0.014	b.d. ^e	b.d.
Na	0.040	n.a.	b.d.	b.d.
K	0.002	n.a.	b.d.	b.d.
Si	0.047	0.046	0.028	0.033
Al	0.028	0.007	b.d.	b.d.
Sr	0.002	n.a.	0.004	0.005
La	0.017	n.a.	b.d.	b.d.
Ce	0.049	n.a.	0.009	0.006
S	0.002	n.a.	0.003	0.003
Nd	0.050	n.a.	n.a.	n.a.
Cations	4.95	7.97	8.00	8.04
Cl	b.d.	0.022	0.019	0.029
F	0.661	1.027	0.968	1.015

^aAnalysis from University of Northern Arizona.

^bAnalysis from University of Hawai'i at Manoa.

^cn.a. = not analyzed.

^dNd₂O₃ estimated from energy dispersive spectrum.

^eb.d. = below detection.

clasts duplicate results from the olivine gabbro; however, several analyses of gabbroic pyroxene from the breccia show a trend toward much higher Fe/Mg (maximum of Fs₆₀ from the breccia, maximum of Fs₃₃ from the olivine gabbro lithology). The trend toward higher Fe/Mg is accompanied by a shift toward Ca-contents near Wo₂₀, intermediate between the high-Ca augite and low-Ca pigeonite compositions characteristic of the olivine gabbro (Fig. 4). Pyroxene with

higher Fe/Mg also tends to be enriched in Ti and depleted in Cr (Fig. 5). Analyses of plagioclase from the gabbroic clasts range in composition from An₉₆ to An₈₀, covering the same range as plagioclase distant from and proximal to residual pockets in the olivine gabbro lithology (Table 5).

Fe-Rich Lithic Clasts: Fayalite-Bearing Gabbroic and Granitic Rocks

Fayalitic olivine, K, Ba-feldspar, and minor whitlockite and apatite are characteristic of the Fe-rich lithic clasts in the breccia (Tables 2, 5, and 7). Hedenbergite, silica, plagioclase feldspar, troilite, and baddeleyite may also be present. The largest, most abundant Fe-rich lithic clasts are composed mostly (>60%) of hedenbergite and fayalite and are referred to here as fayalite gabbros (Fig. 6a); they are unusual gabbros, however, in that the dominant feldspar is K, Ba-feldspar. Other Fe-rich lithic clasts have abundant (>60%) silica +

feldspars, minimal hedenbergite, and significant plagioclase, as well as alkali feldspar (Fig. 6b), and are referred to here as fayalite granites. Abundances of silica, plagioclase, and alkali feldspar vary beyond granitic ratios *sensu stricto*, but the clasts are broadly granitic in composition in that they are enriched in silica and feldspars.

In spite of the range of modal abundances from gabbroic to granitic rocks, mineral textures and compositions in the Fe-rich lithic clasts are similar in many respects. Hedenbergite and fayalite tend to have equant to prismatic, subhedral crystal form, with crystal sizes ranging up to several hundred micrometers across (Figs. 6a and 6b). The K, Ba-feldspar is finer-grained and interstitial to mafic silicates in gabbroic clasts; in granitic clasts, feldspars are intergrown with thin blades of silica (Fig. 6b). Silica in the Fe-rich lithic clasts often has a prismatic shape but appears to be isotropic. Whether or not the isotropic structure of silica is original or a

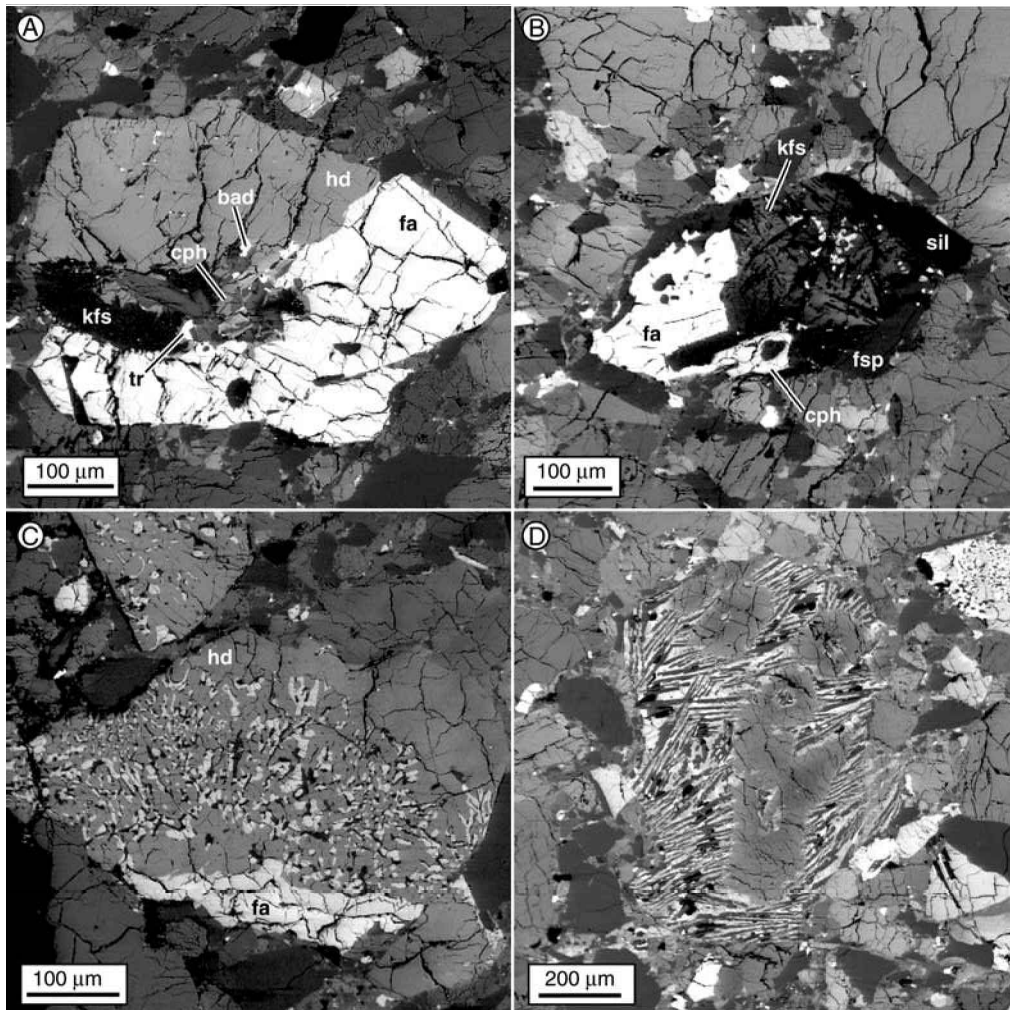


Fig. 6. Backscattered electron images from NWA 773 breccia lithology: a) Fe-rich lithic, gabbroic clast; b) Fe-rich lithic, granitic clast; c) symplectite; d) clast of pyroxene phyric basalt. Mineral abbreviations: bad = baddeleyite; cph = Ca-phosphate; fa = fayalite; fsp = plagioclase feldspar; hd = hedenbergite; kfs = K, Ba-feldspar; sil = silica glass; tr = troilite. The dark gray phase with hedenbergite and fayalite in symplectite (c) is silica.

consequence of shock deformation is not known. Where present, plagioclase feldspar has equant or tabular morphologies and occurs in crystals on the order of 100 μm across. Ca-phosphates are fine-grained with prismatic or anhedral form, and in the fayalite granites, occur as very fine-grained anhedral crystals interstitial to the bladed intergrowths of K, Ba-feldspar and silica (Fig. 6b).

The fayalitic composition of olivine in the Fe-rich lithic clasts constitutes a discontinuous break from the more Mg-rich compositions of olivines from the olivine gabbro lithology and from gabbroic fragments in the breccia (Fig. 3). The hedenbergitic pyroxene is much more Fe-rich than augite and pigeonite characteristic of the olivine gabbro and the most Mg-rich gabbroic clasts in the breccia. However, several analyses of gabbroic pyroxene have intermediate Fe:Mg and Ti:Cr ratios (Figs. 4, 5). Compositions of feldspars from the Fe-rich lithic clasts fall in the same range as those from gabbroic clasts and the olivine gabbro lithology, but on average, are more enriched in alkalis. All 7 analyses of plagioclase from the Fe-rich lithic clasts fall between An₇₂ and An₇₅, compositions enriched in albite compared to plagioclase from the olivine gabbro and the gabbroic clasts. The K, Ba-feldspar in Fe-rich lithic clasts ranges to higher Ba contents (Cs₁₃) than the olivine gabbro K, Ba-feldspar.

Symplectite

Symplectic clasts are composed of silicates similar to the Fe-rich lithic clasts, but with abundant fine-grained intergrowths of symplectic hedenbergite, fayalite, and silica-rich phases (Fig. 6c). The symplectite is characterized by fine-grained, worm-like intergrowths of fayalite and hedenbergite with silica-rich glass or feldspar, \pm Fe, Ti-oxide. Massive ("nonsymplectic") domains of fayalite and hedenbergite occur in the same clasts adjacent to symplectic domains. In addition to these phases, coarse-grained equant apatite and euhedral plagioclase feldspar are present in some symplectic clasts. This occurrence of plagioclase has a composition near An₇₀₋₇₅, similar to plagioclase from the Fe-rich lithic clasts and plagioclase adjacent to the incompatible-element-rich, residual pockets in the olivine gabbro lithology (Table 5). A transitional symplectite texture is present in some hedenbergitic pyroxene crystals, which host multiple, closely-spaced, spherical to irregularly shaped inclusions of fayalite and a silica-rich phase, \pm Fe, Ti-oxide (Fig. 6c).

Symplectic olivine is fayalitic, similar in composition to olivine from the Fe-rich lithic clasts but with a range extending to lower Fe:Mg (Table 2; Fig. 3). Likewise, symplectic pyroxene is generally similar in composition to hedenbergite from the Fe-rich lithic clasts but with a range extending to lower Fe:Mg and Ti:Mg ratios (Table 4; Figs. 4 and 5). Analyses of the silica-rich phase intergrown with symplectic fayalite and hedenbergite yield results ranging from nearly stoichiometric silica to non-stoichiometric Al₂O₃- and K₂O-bearing compositions (Table 5). Because of

the fine grain size, whether the symplectic silica is crystalline or amorphous is difficult to ascertain. The presence of non-stoichiometric, silica-rich material in the symplectite suggests that at least some of the silica-rich phase formed initially as a glass.

Silica Glass

Relatively small angular fragments of silica glass are widespread in the breccia. The silica clasts are typically no more than 100 to 200 μm in longest dimension, and occur as equant and shard-like angular clasts. Some clasts are coarse enough to exhibit isotropic optics in the thin section, indicative of amorphous silica. A few clasts were analyzed and yielded stoichiometric compositions (Table 5), indicating that the silica may have originally been a crystalline phase that was transformed to glass as a result of shock deformation. However, the silica was also possibly an amorphous phase prior to shock.

Pyroxene-Phyric Basalt

A large clast of texturally distinct basalt was identified in one thin section of NWA 773. The clast is characterized by prismatic phenocrysts of pyroxene up to 150 μm in width, and a groundmass of finely-intergrown, elongate pyroxene and feldspar (Fig. 6d). Some pyroxene phenocrysts enclose melt inclusions or channels that might have crystallized in contact with the surrounding groundmass. The pyroxene phenocrysts have BSE-bright, Fe-rich chilled margins along the external crystal faces and along the internal margins against the melt inclusions (Fig. 2).

The pyroxene phenocrysts exhibit a wide range of composition, with both augite and pigeonite present, and some variation in Fe:Mg (Table 4). The augite and pigeonite are more Fe-rich than pyroxenes from the olivine gabbro lithology (Fig. 4), and the augite is enriched in Ti and Cr relative to pyroxene from both the olivine gabbro and gabbro clasts in the breccia (Fig. 5). The major-element zoning of individual pyroxene phenocrysts in this basaltic clast contrasts with the unzoned pyroxenes characteristic of the olivine gabbro lithology, gabbroic clasts, and Fe-rich lithic clasts. The zoned pigeonite-augite phenocrysts with "hollow" central cores and the groundmass "soda-straw" texture of alternating elongate pyroxene and feldspar are similar to the textures observed in low-Ti basalts from Apollo 12 and 15 (Bence et al. 1971; Bence and Papike 1972).

Zoned Pyroxene

One large clast is composed of two very coarse crystals of pyroxene (800 μm across) with zoning and distinct domains of pigeonite and augite (Table 4). The augite exhibits a narrow range of composition with Mg/(Mg + Fe) lower than that of pyroxene from the olivine gabbro lithology and gabbroic clasts in the breccia (Fig. 4). The augite is similar in Wo-En-Fs content to augite from the pyroxene-phyric basaltic

clast (Fig. 4) but contains significantly less Ti and Cr (Fig. 5). Pigeonite is zoned over a range from $Mg/(Mg + Fe) = 0.62$ to 0.25. The Fe-rich pigeonite occurs in patchy, BSE-bright domains on the order of 100 μm across. Some of the Fe-rich patches are cored by tiny BSE-bright inclusions of Fe, Ti-oxide.

Agglutinate

One coarse clast (~400 μm across) and several smaller fragments of lunar agglutinate were identified in the breccia. The agglutinate fragments are characterized by a frothy, isotropic material with discontinuous schlieren and multiple tiny mineral inclusions. Broad-beam EPMA analyses of the largest agglutinate fragment were concentrated on glassy areas within the agglutinate. The results show a narrow range of compositions with significant SiO_2 , Al_2O_3 , and CaO, and minor FeO and MgO (Table 3). The anorthositic composition of the agglutinate glass is in striking contrast to the mafic composition of the olivine gabbro and lithic clasts in the breccia.

Yellow-Green Spherule

One yellow-green spherule in the breccia is nearly circular in the plane of the thin section with a diameter of approximately 180 μm . The spherule is composed of homogeneous-appearing isotropic material with uniform color and is devoid of inclusions and internal structures such as schlieren. Broad beam EPMA analyses indicate that the spherule is also homogeneous in major elements and has an alkali-depleted, basaltic composition with 43 wt% SiO_2 and 15 wt% Al_2O_3 (Table 3). The homogeneity of the composition and the absence of schlieren and inclusions are consistent with a volcanic, rather than an impact-related, origin for the spherule (Delano 1986); however, the spherule is unusually Al_2O_3 -rich in comparison to melt spherules from the Apollo sample collection (Delano 1986; Steele et al. 1992). Using the classification scheme of Neal and Taylor (1992) for mare basalts, the spherule is low in TiO_2 and K_2O , high in Al_2O_3 , and could be classified as "high-Al basalt," similar to basalts from Apollo 14 and Luna 16. However, the spherule Al_2O_3 content is somewhat high, even compared to these high-Al basalts, and Na_2O and K_2O are depleted. The pyroxene phyric melt inclusions in olivine in NWA 773 have comparable Al_2O_3 contents but are much more silica-rich and have an order of magnitude more Na_2O (Table 3). Obvious differences in most major elements distinguish the spherule from the aphyric melt inclusions in olivine and glass from an agglutinate clast in the breccia (Table 3).

A rough fit to the spherule major element composition is approximated by a mixture of 25% agglutinate glass and 75% breccia, suggesting that the spherule may be an impact glass in spite of its homogeneous appearance. Concentrations of SiO_2 , Na_2O , and K_2O in the spherule are all lower than the corresponding values for the calculated mixture. In fact, Na_2O

and K_2O concentrations in the spherule are at or below our EPMA detection limits (Table 3), and the spherule SiO_2 is lower than values associated with regoliths of comparable TiO_2 and FeO contents (Korotev et al. 2000). These observations indicate that the spherule might have been heated to temperatures high enough to homogenize and cause evaporative loss of Si, Na, and K during an impact event (Naney et al. 1976).

WHOLE-ROCK ELEMENTAL AND OXYGEN ISOTOPIC COMPOSITION

Major element concentrations were estimated by modal recombination for the olivine gabbro and fused bead EPMA (FB-EPMA) for the breccia (Table 8). Concentrations of Na_2O , K_2O , CaO, Cr_2O_3 , and FeO were also determined by INAA (Table 9), and comparison of the INAA data with results from modal recombination and FB-EPMA provides some assessment of data quality. The INAA data closely duplicate the FB-EPMA results, showing internal consistency of results for the breccia (Table 8). As might be expected, greater discrepancies separate the modal recombination results from INAA data for the olivine gabbro. The greatest relative discrepancies are for K_2O and Cr_2O_3 , components concentrated in phases that occur in minor abundance. Absolute errors in modal estimates and non-representative sampling for INAA analysis may lead to substantial errors in estimating concentrations of these components. The whole-rock concentrations of Na_2O , CaO, and FeO are controlled by modes of the major silicates. The estimates of the concentrations of these oxides are less sensitive to absolute errors in mode or sampling and exhibit smaller discrepancies (within about 10% relative) between the INAA and modal recombination data (Table 8).

The major element results show low- TiO_2 mafic compositions for both the olivine gabbro and breccia (Table 8). High concentrations of MgO and FeO, coupled with low CaO and Al_2O_3 abundances, suggest an affinity with mare or highland Mg-rich rocks. The olivine gabbro and the breccia have similar concentrations of FeO, but the breccia has lower MgO, consistent with the lower $Mg/(Mg + Fe)$ of mafic silicates in the breccia (Fig. 3).

Taken at face value, the modal recombination and FB-EPMA data suggest that K_2O is more abundant in the olivine gabbro than the breccia (Table 8), but this is probably due to a discrepancy in the two data sets, most likely an overestimate of K-feldspar in the mode. Abundances of K_2O were also analyzed by INAA (Table 8) and indicate the opposite trend, namely that the breccia is more K_2O -rich than the cumulate. We favor the INAA results because these data were collected using the same method, and because other incompatible elements, such as Ba and the rare earth elements (REE), are also enriched in the breccia (Table 9; Fig. 7).

Analyses by INAA and ICP-MS show that incompatible

Table 8. Major element composition (wt%) of NWA 773 olivine gabbro and breccia lithologies.^a

Method	Olivine gabbro		Breccia	
	Modal recombination	INAA	Fused bead EPMA	INAA
SiO ₂	42	–	45.7 ± 0.2	–
TiO ₂	0.4	–	0.84 ± 0.05	–
Al ₂ O ₃	5.3	–	8.16 ± 0.18	–
Cr ₂ O ₃	0.8	0.363 ± 0.004	0.43 ± 0.03	0.402 ± 0.004
FeO	20.5	19.6 ± 0.2	19.8 ± 0.3	19.9 ± 0.2
MnO	0.24	–	0.272 ± 0.009	–
MgO	25.5	–	14.16 ± 0.15	–
CaO	4.8	5.0 ± 0.3	8.92 ± 0.08	8.6 ± 0.3
Na ₂ O	0.15	0.153 ± 0.002	0.216 ± 0.009	0.224 ± 0.003
K ₂ O	0.25	0.073 ± 0.014	0.111 ± 0.008	0.117 ± 0.010
P ₂ O ₅	n.a.	–	0.12 ± 0.02	–
Total	100	–	98.7	–
Mg/(Mg + Fe)	69	–	56.1 ± 0.2	–
Fe/Mn	84	–	72 ± 2	–

^aReported uncertainties for fused bead EPMA are standard deviations of 48 analyses. See the text for the discussion of uncertainties in modal recombination data. INAA data (see Table 9) are shown for comparison. The total of 100 for modal recombination data is a consequence of normalization and does not reflect the accuracy of the compositional estimates.

Table 9. INAA results from NWA 773 olivine gabbro and breccia lithologies and a gabbroic clast from the breccia.^a

Mass (mg)		Olivine gabbro	“Clast” ^b	Breccia ^b	BHVO-1 ^c	
		39.41	14.46	23.47	JSC	Lit
Na ₂ O	wt%	0.153 ± 0.002	0.160 ± 0.002	0.224 ± 0.003	2.30	2.26
K ₂ O	wt%	0.073 ± 0.01	0.066 ± 0.00	0.117 ± 0.010	0.57	0.52
CaO	wt%	5.0 ± 0.3	5.4 ± 0.4	8.6 ± 0.3	10.8	11.4
Sc	µg/g	23.1 ± 0.2	22.2 ± 0.2	38.5 ± 0.4	31.2	31.8
Cr ₂ O ₃	wt%	0.363 ± 0.004	0.238 ± 0.003	0.402 ± 0.004	0.0420	0.042
FeO	wt%	19.6 ± 0.2	18.8 ± 0.2	20.0 ± 0.2	10.8	11.0
Co	µg/g	86.0 ± 0.9	86.9 ± 0.9	61.7 ± 0.7	44.5	45
Ni	µg/g	195 ± 17	219 ± 19	115 ± 16	127	121
Sr	µg/g	40 ± 16	<90	71 ± 16	398	403
Zr	µg/g	157 ± 26	110 ± 24	183 ± 27	181	179
Cs	ng/g	<150	<90	136 ± 21	93	130
Ba	µg/g	147 ± 8	98 ± 14	156 ± 14	130	139
La	µg/g	8.63 ± 0.1	8.54 ± 0.10	12.6 ± 0.1	15.3	15.8
Ce	µg/g	24.1 ± 0.4	23.2 ± 0.4	34.1 ± 0.6	37.5	39
Nd	µg/g	13.6 ± 2.1	15 ± 3	23 ± 4	27	25.2
Sm	µg/g	4.06 ± 0.05	4.05 ± 0.06	6.29 ± 0.08	6.09	6.2
Eu	µg/g	0.359 ± 0.010	0.355 ± 0.008	0.561 ± 0.010	2.07	2.06
Tb	µg/g	0.832 ± 0.025	0.839 ± 0.025	1.40 ± 0.03	0.94	0.96
Yb	µg/g	2.92 ± 0.04	2.85 ± 0.06	5.27 ± 0.08	1.97	2.02
Lu	µg/g	0.406 ± 0.008	0.390 ± 0.010	0.752 ± 0.016	0.278	0.291
Hf	µg/g	3.70 ± 0.0	3.00 ± 0.08	4.70 ± 0.10	4.62	4.38
Ta	ng/g	367 ± 19	372 ± 18	553 ± 18	1150	1230
W	ng/g	nd ^d	nd	470 ± 160	nd	270
Ir	ng/g	<2.5	<3	<3	nd	<i>0.44</i>
Au	ng/g	<1.4	<2.8	<2.1	nd	1.6
Th	µg/g	1.16 ± 0.0	1.26 ± 0.06	1.98 ± 0.08	1.13	1.08
U	ng/g	360 ± 30	320 ± 70	520 ± 60	400	420

^aUncertainties are 1σ; upper limits are 2σ.

^bSee Appendix for ICP-MS data.

^cAn average of BHVO-1 analyzed along with the NWA 773 samples is shown along with the book values from Govindaraju (1994), which are **recommended**, proposed, or *information* values.

^dnd = upper limits not calculated.

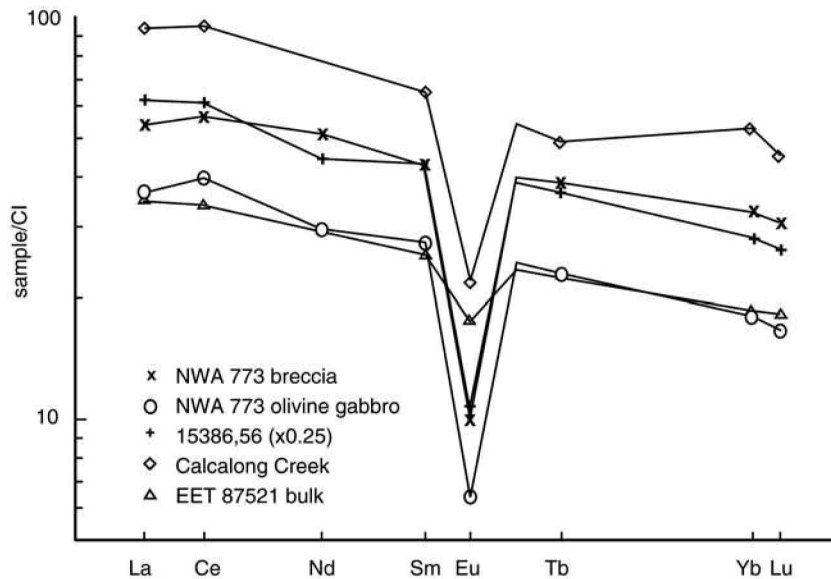


Fig. 7. Rare earth element concentrations of NWA 773 (normalized to CI chondrites) compared with selected lunar samples.

elements such as Zr, Hf, Th, U, and the REE occur in higher concentrations in the breccia than the olivine gabbro (Tables 9 and A1). The breccia is also relatively enriched in Sc, possibly reflecting the high model abundances of pyroxenes. In contrast, the olivine gabbro yielded higher concentrations of the compatible elements Co and Ni. Chromium appears to be more abundant in the breccia, but this is somewhat paradoxical because our modal estimates suggest that the mode of chromite is higher in the olivine gabbro (Table 1). However, the discrepancy between modal recombination and INAA Cr_2O_3 results (Table 8) suggests that our modal estimate of chromite in the olivine gabbro might be erroneously high. Alternatively, chromium abundances may vary in different portions of the olivine gabbro. In general, however, the higher concentrations of incompatible elements in the breccia suggest that breccia clasts are more “evolved” in the igneous sense than the olivine gabbro. This is consistent with the modal data (lower olivine and greater silica abundances of the breccia) and mineral compositions (higher K and Ba in breccia alkali feldspar and lower $\text{Mg}/(\text{Mg} + \text{Fe})$ in mafic silicates in the breccia).

Rare earth element (REE) patterns for the breccia and olivine gabbro are parallel and reflect the higher incompatible element abundances of the breccia (Fig. 7). Both patterns are LREE-enriched with slight downward deflections from Ce to La and deep negative Eu anomalies. Similar results have been reported by Korotev et al. (2002). Light rare earth enrichments and negative Eu anomalies are typical of the lunar KREEP component (Papike et al. 1998), and LREE profiles with slight downward deflections in Ce have recently been identified in a variety of lunar mafic rocks (Tanimizu and Tanaka 2002). The concentrations of most REE in the NWA 773 olivine gabbro are similar to those of lunar

meteorite Elephant Moraine 87521, which is thought to have a mare origin (Delaney 1989; Warren and Kallemeyn 1989), but NWA 773 has a much deeper Eu anomaly (Fig. 7). The LREE-rich profile of lunar highlands meteorite Calalong Creek is similar to that of NWA 773 but is enriched in REE by a factor of about 2 over REE concentrations in the NWA 773 breccia. Most of the low- TiO_2 mare basalts have flat or somewhat depleted LREE trends (Papike et al. 1998), which contrast with the LREE-enriched pattern of NWA 773. Some of the high-Al basalts from Apollo 14 are exceptions: the Group 2 Apollo 14 basalts (Dickinson et al. 1985), in particular, show an LREE-enriched pattern with concentrations similar to those determined for the NWA 773 breccia.

Whole-rock oxygen isotopic analyses yield compositions of $\delta^{18}\text{O} = +4.99\text{‰}$ and $\delta^{17}\text{O} = +2.50\text{‰}$ for the olivine gabbro, and $\delta^{18}\text{O} = +4.93\text{‰}$ and $\delta^{17}\text{O} = +2.60\text{‰}$ for the breccia. These values are in the range of previously identified lunar samples (Fig. 8). Similar oxygen isotopic compositions for the 2 lithologies are consistent with the notion that the breccia is dominated by fragments from the olivine gabbro and related rocks.

NOBLE GASES

Table 10 gives the results of the noble gas analyses. Preliminary data were given in an abstract by Eugster and Lorenzetti (2001). Partitioning into the cosmogenic (c), radiogenic (r), and trapped (tr) components was carried out with the following assumptions: $(^4\text{He}/^3\text{He})_c = 5.2$, $(^{20}\text{Ne}/^{21}\text{Ne})_c = 0.9$, $(^{21}\text{Ne}/^{22}\text{Ne})_c = 0.83$, $(^{21}\text{Ne}/^{22}\text{Ne})_{tr} = 0.0325$, $(^{36}\text{Ar}/^{38}\text{Ar})_c = 0.65$, and $(^{36}\text{Ar}/^{38}\text{Ar})_{tr} = 5.32$. The following assumptions were obtained from the results of Y-793274

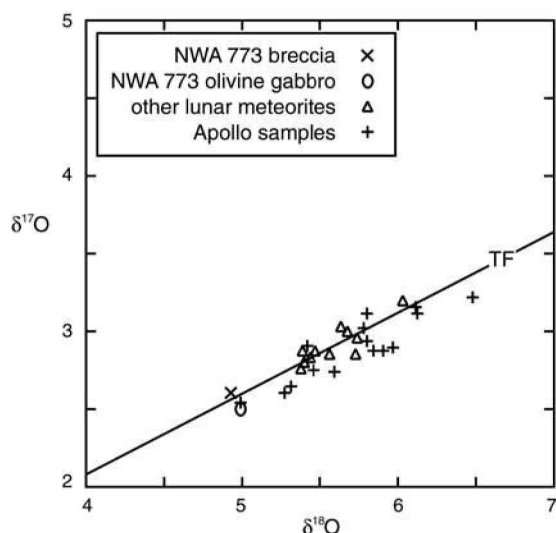


Fig. 8. Whole-rock oxygen isotopic compositions of NWA 773 breccia and olivine gabbro, and other lunar rocks (Clayton and Mayeda 1975, 1996). Compositions are reported in $\delta^{17}\text{O}$ and $\delta^{18}\text{O}$ relative to standard mean ocean water (SMOW) in parts per thousand. Terrestrial fractionation (TF) line (Clayton 1993) is plotted for reference.

(Eugster et al. 1992): $(^3\text{He}/^{21}\text{Ne})_c = 0.73$ and $(^{38}\text{Ar}/^{21}\text{Ne})_c = 1.98$. For the breccia samples, $^4\text{He}_{\text{tr}}$ was calculated by subtracting radiogenic and cosmogenic ^4He from the measured ^4He concentration. We adopted 0.52 ppm U and 1.98 ppm Th (Table 9) and a gas retention age of 2.8 Ga (from Y-793274). In the following, we will consider the trapped noble gases to be of solar origin as numerous authors have shown for lunar surface material (cf. Eberhardt et al. 1970; Hohenberg et al. 1970). Table 11 gives the concentrations and composition of the cosmogenic and solar noble gases. The data show that the finest grain size fraction is not enriched in the solar noble gases. Such an enrichment is expected for a surface correlated component. Thus, the trapped $^{40}\text{Ar}/^{36}\text{Ar}$ ratio that is diagnostic for a lunar origin of a meteorite could not be derived. However, the solar ratio $^4\text{He}/^{20}\text{Ne} = 7.2 \pm 0.7$ indicates that NWA 773 is of lunar origin: the range for the

solar $^4\text{He}/^{20}\text{Ne}$ ratio for lunar meteorites is 3.7 to 8.8, while all solar gas-rich meteorites of non-lunar origin have $^4\text{He}/^{20}\text{Ne} > 80$. Furthermore, the solar $^{20}\text{Ne}/^{22}\text{Ne}$ ratio, as well as the abundances of $^{21}\text{Ne}_c$ and solar ^{20}Ne in NWA 773 are similar to those in QUE 94281, another lunar meteoritic regolith breccia.

The cosmic ray exposure (CRE) history of lunar meteorites consists essentially of three periods: 1) one or more exposure irradiation periods on the moon, each at a certain depth in the regolith; 2) an irradiation during transit to Earth; and 3) the time elapsed between arrival on Earth and the meteorite's recovery. These times can only be defined based on the activities of several radionuclides. The concentrations of the stable cosmogenic noble gas nuclei allow us, however, to calculate the total CRE time at an average shielding depth. Here, we derive the production rates for a 4π -exposure of the olivine gabbro fraction using the method of Eugster and Michel (1995), inserting the target element abundances given in Table 8, and not taking into account a shielding correction.

This procedure results in a CRE age of 5.2 ± 0.8 Ma (Table 12). This is the ejection age of NWA 773 if the olivine gabbro fraction was not exposed to cosmic rays prior to ejection on the moon. If there was a pre-exposure of unknown duration for the olivine gabbro, the ejection age is more recent than 5.2 ± 0.8 Ma. Assuming a 4π -exposure also for the breccia fraction, we obtain a travel time of 68 Ma. As the meteoroid after ejection obviously consisted of both fractions, they must have the same Moon—Earth travel time. Consequently, the breccia fraction must have been pre-exposed on the moon. Because the production rates in the lunar regolith (2π -exposure) are about half of those in free space (4π -exposure), the duration of the lunar regolith exposure was 136 Ma. When this pre-exposure occurred and when the olivine gabbro and breccia fractions were compacted cannot be determined from our data. The fact that the breccia material consists of grains loaded with solar wind gases supports an exposure on the moon. The olivine gabbro contains a small addition of solar noble gases: the concentration (in units of 10^{-8} cm³ STP/g) of solar ^{20}Ne is 7.2,

Table 10. Results of He, Ne, and Ar measurements of NWA 773 (concentrations in 10^{-8} cm³ STP/g).

Sample (weight)	^4He	^{20}Ne	^{40}Ar	$^4\text{He}/^3\text{He}$	$^{20}\text{Ne}/^{22}\text{Ne}$	$^{22}\text{Ne}/^{21}\text{Ne}$	$^{36}\text{Ar}/^{38}\text{Ar}$	$^{40}\text{Ar}/^{36}\text{Ar}$
Breccia								
340–750 μm (15.84 mg)	181,000 $\pm 7,000$	20,400 ± 600	5470 ± 160	2580 ± 70	12.93 ± 0.13	23.7 ± 0.4	5.27 ± 0.05	2.21 ± 0.03
35–340 μm (15.01 mg)	192,000 $\pm 7,000$	22,300 ± 500	5960 ± 160	2470 ± 50	12.89 ± 0.13	23.4 ± 0.3	5.27 ± 0.04	2.25 ± 0.03
< 35 μm (14.65 mg)	175,000 $\pm 7,000$	16,900 ± 500	5050 ± 160	2240 ± 50	12.94 ± 0.13	22.8 ± 0.3	5.28 ± 0.04	2.30 ± 0.03
Olivine gabbro								
(18.40 mg)	16,500 ± 600	8.8 ± 0.3	1540 ± 40	3400 ± 300	3.5 $\pm 0.$	1.42 ± 0.20	1.83 ± 0.03	1350 ± 30

Table 11. Cosmogenic and solar (trapped) noble gases of NWA 773 samples. Concentrations in $10^{-8} \text{ cm}^3 \text{ STP/g}^{\text{a}}$

Sample	Cosmogenic		Solar			
	^{21}Ne	^{38}Ar	^{20}Ne	$^4\text{He}/^{20}\text{Ne}$	$^{20}\text{Ne}/^{36}\text{Ar}$	$^{20}\text{Ne}/^{22}\text{Ne}$
Breccia						
340–750 μm	15.9	–	20,410	6.8	8.3	13.08
35–340 μm	18.3	–	22,230	6.8	8.5	13.05
<35 μm	15.4	–	16,900	7.9	7.8	13.12
Average of three breccia samples	16.5	–	19,850	7.2	8.2	13.08
Olivine gabbro	1.73	0.47	7.2	–	8.6	–

^aExperimental errors (2σ): ^{21}Ne , ^{38}Ar , and $(^4\text{He}/^{20}\text{Ne})_{\text{tr}}$ – 10%; ^{20}Ne and $(^{20}\text{Ne}/^{36}\text{Ar})_{\text{tr}}$ – 4%; and $(^{20}\text{Ne}/^{22}\text{Ne})_{\text{tr}}$ – 1.5%.

Table 12. Production rates and CRE ages of NWA 773.

Sample	P_{21}	P_{38}	T_{21}	T_{38}	T_{ave}
	$10^{-8} \text{ cm}^3 \text{ STP/g Ma}$		Ma		
Cataclastic breccia fraction	0.121 ^a	–	136 ^b		$136 \pm 20 (2\sigma)^{\text{b}}$
Olivine gabbro	0.335 ^c	0.089 ^c	5.2 ^d	5.3 ^d	$5.2 \pm 0.8 (2\sigma)^{\text{d}}$

^aProduction rate for 2π -exposure.

^bExposure time on the moon.

^cProduction rate for 4π -exposure.

^dUpper limit for exposure time in Moon-Earth transit.

versus 19,850 for the breccia. This low amount may be due to traces of breccia grains in the olivine gabbro separate that we analyzed.

The ^{40}Ar is a mixture of radiogenic, trapped, and cosmogenic Ar. For the olivine gabbro, the contributions of Ar_{tr} and Ar_{c} are calculated to be about 0.06% of the total ^{40}Ar (Table 10). For the breccia fraction, the amount of $^{40}\text{Ar}_{\text{r}}$ cannot be determined precisely. For the olivine gabbro, we observe $1530 \times 10^{-8} \text{ cm}^3 \text{ STP/g } ^{40}\text{Ar}_{\text{r}}$ and 0.073% K_2O (Table 9) and calculate a K-Ar age of $2.75 \pm 0.30 \text{ Ga}$. This age is essentially the same as that of the lunar meteorite Y-793274. The geologic significance of this age is not known. If, however, it is a crystallization age, then the olivine gabbro post-dates much of the igneous evolution of the moon, including the lunar magma ocean, overturn of the cumulate sequence, and the main pulse of mare volcanism (Hess and Parmentier 1995; Shearer and Papike 1999).

DISCUSSION

Lunar Origin

Igneous textures of the olivine gabbro and of many clasts in the breccia indicate that NWA 773 originated from a differentiated parent body, and the oxygen isotopic composition independently rules out all potential known parent bodies other than the earth, the moon, and enstatite chondrite-like asteroids. The abundance of Fe in solid solution with Mg in olivine and pyroxene demonstrates that NWA 773 did not originate from an enstatite chondrite-like parent body. The presence of agglutinate fragments in the breccia indicate that NWA 773 originated from a parent body without an atmosphere, ruling out a terrestrial origin, and

leaving the moon as the sole candidate among known planets and asteroids for the parent body of NWA 773.

A comparison of key geochemical parameters with samples from the Apollo and Luna missions and previously identified lunar meteorites document that NWA 773 originated on the moon. Ratios of Fe/Mn in NWA 773 olivine and pyroxene are characteristic of lunar rocks (Fig. 3), and the LREE-enriched, Eu-depleted REE pattern is typical of lunar rocks with a KREEP component (Fig. 7; Bridges et al. 2002; Korotev et al. 2002). Trapped $^4\text{He}/^{20}\text{Ne}$ and $^{20}\text{Ne}/^{36}\text{Ar}$ values of the NWA 773 breccia (Table 11) are similar to previously identified lunar meteorites and distinct from gas-rich meteorites of non-lunar origin. Other observations consistent with a lunar origin for NWA 773 include the presence of Fe-metal, ilmenite, and troilite; the apparent absence of ferric iron from pyroxene and spinel; the F-rich composition of apatite; and the Ba-rich composition of K-feldspar.

Petrogenesis: Olivine Accumulation in the Olivine Gabbro

The texture of the olivine gabbro is dominated by the loose network of coarse olivine crystals (Fig. 1), and the other phases can all be described in the context of a rock that accumulated olivine. In general, textures suggest the following crystallization sequence: olivine, pigeonite, augite, plagioclase, and K, Ba-feldspar with residual Ca-phosphates, ilmenite, troilite, and metal. Titaniferous chromite tends to occur along olivine grain boundaries, indicating that it post-dated olivine. The crystallization sequence among the mafic silicates is indicated by the occurrence of olivine rimmed by pigeonite, which is rimmed in turn by augite, and by the absence of conflicting crystal-rimming relationships (Fig. 1). Plagioclase tends to occur in the interstices between mafic

silicates suggesting that it crystallized after olivine and pyroxene. A variety of textural relationships exist, however, and undoubtedly, there was some overlap during crystallization of the pyroxenes, plagioclase feldspar, and residual minerals.

The interpretation, based on textures, that most of the pyroxene in the olivine gabbro crystallized prior to feldspar is supported by the low Ti/Al ratios in pyroxene. Pyroxene with Ti/Al near 1/4 can be attributed to sub-equal proportions of the cation substitutions $\text{TiAl}^{\text{IV}}_2\text{Mg}_{-1}\text{Si}_{-2}$ (coupled Ti-exchange) and $\text{Al}^{\text{VI}}\text{Al}^{\text{IV}}\text{Mg}_{-1}\text{Si}_{-1}$ (Tschermak exchange) into a "quadrilateral" pyroxene such as $\text{CaMgSi}_2\text{O}_6$ (Bence et al. 1971; Thompson 1982), while Ti/Al values near 1/2 can be attained if all of the Al present in pyroxene is coupled with Ti to maintain charge balance. In the olivine gabbro, most pyroxene Ti/Al values are near or below 1/4 and all are below 1/2. In studies of lunar mafic rocks from Apollo 12 (Bence et al. 1970; Bence and Papike 1972) and lunar basalt NWA 032 (Fagan et al. 2002), Ti/Al values near 1/4 are associated with crystallization prior to feldspar, and Ti/Al values near 1/2 are interpreted as a consequence of co-crystallization with feldspar. We suggest a similar trend for NWA 773. Values of Ti/Al near 1/4 for most (but not all) of the pyroxene in the olivine gabbro are consistent with crystallization of most (but not all) of the pyroxene prior to the onset of feldspar crystallization. Pyroxene from many of the gabbroic clasts in the breccia, much of the zoned pyroxene clast, and phenocrysts from the pyroxene-phyric basalt clast also have Ti/Al values near 1/4 (Fig. 5). In contrast, pyroxenes from the Fe-rich lithic, symplectite, and transitional symplectite clasts have Ti/Al values clustering near 1/2 (Fig. 5) and have textures indicating crystallization after the onset of feldspar crystallization.

The occurrence of separate grains of compositionally distinct pigeonite and augite indicates that either: a) the olivine gabbro cooled slowly enough so that the pyroxenes completely exsolved from each other; or b) pigeonite and augite crystallized separately from a melt. We favor the latter interpretation because the very slow cooling required for complete separation of pigeonite and augite should also result in thick (>1 μm) exsolution lamellae of Ca-poor orthopyroxene from pigeonite (e.g., Arai et al. 1996; however, see Korotev et al. [2002], who identified exsolution lamellae in NWA 773). The polyhedral to "hopper" texture of olivine suggests that the olivines grew at cooling rates slower than about 5°C/hr, as faster cooling rates would produce more elongate crystals with higher surface areas (Donaldson 1976).

Augite and pigeonite coprecipitate from olivine-saturated liquids over a wide pressure range from surface conditions to pressures as high as 15 kbar for melts with $\text{MgO}/(\text{MgO} + \text{FeO}) = 0.5$ (Longhi and Bertka 1996). After crystallization from liquid, the pyroxenes cooled and equilibrated at ~1150°C (assuming $P = 1$ bar; Lindsley 1983; Sack and Ghiorso 1994). Pyroxene crystallization in the olivine gabbro did not

fractionate the liquid significantly in $\text{Mg}/(\text{Mg} + \text{Fe})$, but did fractionate the liquid $\text{Ti}/(\text{Ti} + \text{Cr})$ (Fig. 5).

Textures and pyroxene Ti:Al ratios indicate that most pyroxene crystallization was completed by the time feldspar started to crystallize. Most plagioclase crystallized with a composition near An_{90} , but as crystallization continued and melt pockets became isolated, Ab- and Or-contents of plagioclase increased. Isolated residual melt pockets are represented by the K, Ba-feldspar with splays of Ca-phosphates, ilmenite, troilite, and metal.

The residual melt pockets, though minor in mode, may have a significant effect on whole-rock trace element chemistry because the olivine gabbro does not have an incompatible element pattern typical of cumulate rocks. The REE abundances and pattern (Fig. 7) and the abundances of Hf, Ta, Th, and U are all unusually high for a cumulate. The most incompatible elements have the highest abundances, with La, Hf, Th from 36 to 39 \times CI chondrite, while the less incompatible elements show smaller enrichments, with Yb of 18 \times CI, and Sc, Eu of 4 to 6 \times CI. This demonstrates that the incompatible trace element contents are dominated by a melt component. This conforms with the texture, which indicates that only olivine is a likely cumulus phase and that the modal abundance of olivine is roughly 55% of the rock.

Traditionally, cumulates have been interpreted to form as a consequence of crystal settling or floating in a silicate liquid, and on a very large-scale, cumulate differentiation by plagioclase floating and mafic silicates sinking in a lunar magma ocean has been invoked as a major mechanism for differentiation of the moon (Warren 1985). However, work on terrestrial layered mafic intrusions makes it clear that cumulate textures may form from processes other than crystal settling, involving differential crystal nucleation and growth rates, in situ crystallization fronts, filter pressing of residual liquids, and differentiation during magmatic flow (McBirney and Noyes 1979; McBirney and Hunter 1995). Even in the case of well-exposed cumulate intrusives on Earth, the origin of cumulate textures can be controversial, and without a field context, we do not expect to readily establish the origin of cumulate textures in NWA 773. However, crystal settling of olivine remains a viable model.

Shared Magmatic Origin of Cumulate Olivine Gabbro and Breccia Clasts

The breccia comprises several different rock types, but many appear to be from the cumulate olivine gabbro or more Fe-rich differentiates. The olivine gabbro and gabbroic clasts in the breccia share similar mineral assemblages, mineral compositions and textures, and both have olivines with characteristic andesitic melt inclusions. Several pyroxene and olivine analyses from the gabbroic clasts essentially match those from the olivine gabbro in major element composition (Figs. 3 and 4) and, for the pyroxenes, Ti, Al, and Cr

elemental ratios (Fig. 5). Oxygen isotopic compositions of the breccia and cumulate plot close together within the range of values determined for lunar samples (Fig. 8), suggesting that the breccia and cumulate are derived from a similar local source on the moon. Related origins for the cumulate olivine gabbro and most clasts in the breccia are also implied by the parallel REE patterns (also see Korotev et al. 2002). The similar patterns suggest that REE concentrations of both lithologies are dominated by the same REE-rich minerals (most likely whitlockite) that crystallized from related liquids. The higher bulk REE concentrations of the breccia can be explained as a result of the presence of clasts that crystallized from differentiated liquids.

Pyroxene compositions from the gabbroic clasts extend to lower Mg/(Mg + Fe) and higher Ti/(Ti + Cr) values on simple trends from compositions characteristic of the olivine gabbro (Figs. 4 and 5), as would be expected for a fractionating igneous system (Arai et al. 1996, 2002). In contrast to the broad continuous range in Mg/(Mg + Fe) for pyroxene, olivine from the gabbroic clasts exhibits only a limited trend toward lower Mg/(Mg + Fe). A compositional gap separates olivine in the gabbroic clasts from the olivine observed in Fe-rich lithic and symplectic clasts (Fig. 3). This compositional gap can be explained as a consequence of: 1) early crystallization of olivine, which then ceased to crystallize while pigeonite and augite grew in the melt; followed by 2) Fe-enrichment into the "forbidden zone" of the pyroxene quadrilateral, where pigeonite gives way to fayalite + silica + hedenbergitic pyroxene (Lindsley and Munoz 1969). In contrast to the cumulate olivine gabbro stage of crystallization, clasts in the breccia appear to have formed from a magmatic system in which mafic silicates fractionated the remaining melt to extremely low Mg/(Mg + Fe) and high Ti/(Ti + Cr) (Figs. 3, 4, and 5). As the system became Fe-rich, pigeonite gave way to Ca-rich clinopyroxene, fayalitic olivine, and a SiO₂-rich phase.

Late-stage differentiates are represented by fayalitic rocks, including the symplectites, fayalite gabbros and fayalite granites. The pyroxenes in these clasts have low Mg/(Mg + Fe) and high Ti/(Ti + Cr), indicative of crystallization from evolved liquids, and Ti/Al ratios in excess of 0.5, suggestive of crystallization after the onset of feldspar crystallization. Plagioclase feldspar in the symplectic clasts is relatively An-poor (An ~70), and the K, Ba-feldspar with the highest BaO contents analyzed are from Fe-rich lithic clasts, also indicating that the symplectites and Fe-rich lithic clasts formed from incompatible-element-rich liquids. This inference is supported by the identification of baddeleyite in one of the fayalite gabbro fragments. Fayalite-bearing granitic clasts are not abundant, but their presence suggests that some residual liquids reached alkali- and silica-rich compositions after extreme iron-enrichment from crystallization of the olivine-gabbro/gabbro/fayalitic-rock sequence. Silica clasts, though minor in mode (Table 1), are

widespread in the breccia and may be fragments of SiO₂-rich rocks from late stages of the olivine-gabbro/gabbro/fayalitic-rock sequence.

Iron-rich symplectites have been observed in other lunar samples (Koeberl et al. 1993; Yanai and Kojima 1991) and, in some cases, may form during the breakdown of pyroxferroite to fayalite + silica. In NWA 773, the presence of K₂O- and Al₂O₃-bearing non-stoichiometric silica-rich glass as a phase in the symplectite is not consistent with an origin by the breakdown of a pre-existing stoichiometric solid. Rather, the symplectite in NWA 773 appears to have formed from direct crystallization, or quenching, from one or more liquids. Immiscible liquids in FeO-rich silicate systems have been identified in experiments and in lunar samples (Roedder and Weiblen 1971; Rutherford et al. 1974; Roedder 1978; Ryerson and Hess 1978; Taylor et al. 1980; Shearer et al. 1997; Jolliff et al. 1999) and probably exsolved during late-stage differentiation of Fe-rich gabbroic rocks in NWA 773. Immiscible liquids, rapid crystal growth rates, and relatively slow diffusion rates of cations in liquids are some of the factors that may have led to the symplectic texture in NWA 773.

The presence of 2, possibly immiscible, silicate liquids during earlier stages of igneous differentiation is suggested by the andesitic and silica-rich melt inclusions in olivine from the cumulate olivine gabbro. Some broad beam analyses of the silica-rich inclusions overlapped with Ca-phosphate crystals (internal to the inclusion) resulting in high P₂O₅ in individual analyses, but in general, P₂O₅ concentrations are consistently higher in the andesitic inclusions (Table 3). These results, with the more SiO₂-poor composition enriched in P₂O₅, are consistent with the 2 sets of melt inclusions related by immiscibility rather than crystal fractionation (Ryerson and Hess 1978). Both sets of melt inclusions are unusually SiO₂-rich to be trapped in such an olivine-rich rock, and their compositions may reflect post-trapping alteration and reaction with olivine host crystals (Danyushevsky et al. 2002; Norman et al. 2002).

FeO-Enrichment Trend and Contrast with SiO₂-Enrichment in 15405

The cumulate olivine gabbro lithology and gabbroic, Fe-rich lithic, and symplectic clasts from the breccia can be interpreted as a suite from a mafic igneous system that was characterized by Fe-enrichment to extremely low values of Mg/(Mg + Fe). Some granitic rocks formed after the Mg/(Mg + Fe) of residual liquids reached values near zero. This Fe-enrichment trend contrasts with KREEP-rich fragments identified in lunar breccia 15405 (Ryder 1976). Clasts of KREEP basalt, quartz monzodiorite, and granite in 15405 were interpreted by Ryder as fragments of a composite magmatic system in which monzodiorite and, subsequently, granite were produced by crystal fractionation from an original magma with a composition similar to the KREEP

basalt. Pyroxenes in 15405 reached $Mg/(Mg + Fe)$ as low as about 0.30, significantly fractionated with respect to pyroxenes from the basalt clasts in the breccia but far from the extreme Fe-rich compositions found in NWA 773.

Of course, sample 15405 and NWA 773 are breccias and cannot be taken as complete sample suites from igneous bodies. But, if the rock fragments are representative of the magmatic units from which they come, then they show a marked contrast in differentiation. Sample 15405 reflects a trend of increasing silica-content with moderate Fe-enrichment, while NWA 773 reflects an extreme Fe-enrichment trend. These trends are comparable, in a broad sense, to the terrestrial silica-enrichment (or “Bowen”) trend associated with calc-alkaline magmas and the Fe-enrichment (or “Fenner”) trend associated with tholeiitic mafic bodies such as the Skaergaard intrusion (Brown and Vincent 1963; also see McBirney 1993). In terrestrial systems, the difference between these trends has been associated with variations in $f(O_2)$: high oxygen fugacities can lead to silica enrichment, as Fe is partly oxidized to the ferric form and is precipitated in oxide minerals in addition to mafic silicates (e.g., Yagi and Takeshita 1987); under low oxygen fugacities, most Fe is ferrous and precipitates in mafic silicates that become more Fe-rich with fractionation. In a lunar setting, this explanation does not hold because of the absence of ferric iron. The extent of Fe-enrichment may still have been controlled by oxygen fugacity but in the opposite sense to that on Earth, namely, a relatively high lunar oxygen fugacity may have limited the precipitation of Fe in metal or sulfides, resulting in more extreme Fe-enrichment in the silicates (Snyder et al. 1999a).

Alternatively, the contrast between silica-enrichment in 15405 and iron-enrichment in NWA 773 may have stemmed from differences in dynamics that led to more effective isolation of residual liquid in the NWA 773 magmatic system. Cumulate processing in the NWA 773 system may have depleted residual liquids in $Mg/(Mg + Fe)$, leading to a broad range of lower $Mg/(Mg + Fe)$ values in late differentiates. A wide range of compositions could have crystallized in a small spatial domain, if the magmatic body was relatively small, such as a sill or ponded lava flow (Helz 1987; Shirley 1987), or if multiple packets of magma underwent differentiation independently, as is found in terrestrial layered mafic intrusions (Kruger and Marsh 1985; Boudreau and McBirney 1997; McBirney and Nicolas 1997) and ophiolitic gabbros (Springer 1980; Pallister and Hopson 1981).

Exotic Clasts in the Breccia

Some clasts in the breccia appear to be unrelated to magmatic evolution of the olivine-gabbro/gabbro/fayalitic-rock trend. Pyroxene phenocrysts from the phyric basalt clast (Fig. 6) are enriched in Ti, Al, and Cr compared to clasts from the olivine-gabbro/gabbro/fayalitic-rock suite (Table 4). These pyroxene phenocrysts have distinct $Ti/(Ti + Cr)$ and

$Mg/(Mg + Fe)$ values (Fig. 5), indicating that the high concentrations of Ti, Al, and Cr are not due to differentiation from the olivine-gabbro/gabbro/fayalitic-rock trend (Fig. 5). This clast probably originates from a mare basalt.

The composition of the agglutinate glass is anorthositic (Table 3), distinctly enriched in CaO and Al_2O_3 , and depleted in FeO + MgO compared to the olivine gabbro and lithic breccia fragments. Agglutinate glass is thought to form from fusion of the finest fraction of regolith during meteorite and micrometeorite bombardment (Simon et al. 1985), and thus, may not be precisely representative of the “whole-rock” composition of the regolith from which it forms. In this case, however, the contrast between compositions of the agglutinate glass and lithic fragments is so strong that derivation of the agglutinate from a regolith composed solely of the olivine gabbro lithology and gabbroic and fayalitic clasts from the breccia is untenable. The agglutinate composition indicates an origin from highland anorthosites or related rocks.

The yellow-green spherule also probably represents a lithologic unit that did not form from magmatic evolution of the olivine-gabbro/gabbro/fayalitic-rock series. The spherule is enriched in Al_2O_3 at a SiO_2 -content comparable to that of the olivine gabbro (Tables 3 and 8); thus, removing cumulate olivine from the olivine gabbro composition cannot produce the composition of the spherule. The spherule is enriched in Al_2O_3 and depleted in SiO_2 relative to both sets of melt inclusions in olivine and appears unrelated by any simple fractionation relationship to either set of inclusions.

As discussed previously (Mineralogy and Textures—Breccia Lithology), the spherule may be an impact glass from a mixture of the breccia and anorthositic highland material. The aluminous compositions of the spherule and agglutinate are significant because they indicate a highland component in the NWA 773 breccia.

Comparison with Other Lunar Rocks

The geochemical data compiled during this study clearly indicate a lunar origin of NWA 773, but how this meteorite fits with previously identified lunar rocks is less clear-cut. The deep negative Eu anomaly indicates that NWA 773 was derived from a Eu-depleted source, commonly inferred to be a consequence of plagioclase fractionation. For lunar rocks, the Eu-depletion is associated with a residual liquid (KREEP, or urKREEP for a hypothetical liquid closely associated with the lunar magma ocean) fractionated by the sinking of mafic silicates and the flotation of an anorthosite-rich crust during a primordial lunar magma ocean (Warren 1985; Warren and Kallemeyn 1993b; Shearer and Papike 1999). The Eu-depletion in NWA 773, coupled with its mafic major element composition, indicate that NWA 773 was extracted from mafic or ultramafic material that post-dated plagioclase fractionation in the lunar magma ocean.

The most obvious set of mafic lunar rocks that post-dated the magma ocean are the mare basalts, but as discussed previously, most mare basalts from the Apollo and Luna missions have flat or depleted LREE patterns distinct from the LREE-enriched pattern of NWA 773. Some of the Apollo 14 high-Al basalts are also LREE enriched (Dickinson et al. 1985), but these rocks are distinctly more aluminous than the NWA 773 olivine gabbro and breccia and do not make a good match for NWA 773. However, the similar REE patterns suggest that NWA 773 and the high-Al basalts originated from liquids that melted with or assimilated a lithology with elevated incompatible elements similar to KREEP. Whole-rock and mineral REE analyses reported by others also suggest that at least some of the parent material of NWA 773 had a KREEP-like trace element pattern (Bridges et al. 2002; Korotev et al. 2002). A pyroxene-phyric basaltic clast in the NWA 773 breccia has distinctive textures similar to pigeonite basalts from Apollo 12 and 15, and this clast probably originated from the lunar maria. However, as discussed above (Exotic Clasts in the Breccia), pyroxene from this clast deviates from compositional trends identified in other pyroxenes from the olivine gabbro and breccia, and the clast appears to be unrelated to the olivine gabbro and majority of lithic fragments in the breccia.

Several lunar meteorites share a mafic composition and LREE-enriched pattern generally similar to NWA 773. Lunar meteorites with whole-rock $\text{Al}_2\text{O}_3 < 20$ wt% and $\text{La/Yb} > 1.9$ include: Y-793274 and QUE 94281 (Jolliff et al. 1998); EET 87521 and EET 96008 (Delaney 1989; Warren and Kallemeyn 1989; Snyder et al. 1999a); Northwest Africa 032 (Fagan et al. 2002); and Dhofar 287 (Taylor et al. 2001). In fact, it has been pointed out (Snyder 1999b) that all the analyzed lunar mafic meteorites are LREE-enriched except for the coarse-grained non-brecciated Y-793169 and A-881757 (Koeberl et al. 1993; Warren and Kallemeyn 1993a). The LREE-enrichment of lunar mafic meteorites is not due solely to physical mixing of highland components in breccias because NWA 032 is an unbrecciated basalt. The analysis of Dho 287 by Taylor et al. (2001) is of a basalt fragment that comprises much of the meteorite, and the unbrecciated olivine gabbro lithology of NWA 773 also yields a LREE-enriched pattern. In addition to the similarity in REE, several of these meteorites, including EET 87521, QUE 94281, EET 96008, and Y-981031, also have clasts with highly evolved hedenbergite + fayalite + silica-rich phase assemblages similar to those that occur in the NWA 773 breccia (Delaney 1989; Arai and Warren 1999; Arai et al. 2002; Jolliff et al. 1998; Snyder et al. 1999a).

In spite of these similarities, it is unlikely that any previously identified lunar meteorite is a pair of NWA 773. The negative Eu anomaly of NWA 773 ($\text{Sm}/\text{Eu} = 11.2$ for the olivine gabbro, 11.3 for the breccia) is much deeper than that of the other lunar mafic meteorites; among the meteorites mentioned above, NWA 032 has the second deepest Eu

anomaly with $\text{Sm}/\text{Eu} = 6.0$ (Fagan et al. 2002), nearly half of the value for NWA 773. Furthermore, O-isotopic compositions of the NWA 773 gabbro and breccia differ from those of other lunar meteorites (Fig. 8).

The Mg-suite or Mg-rich nonmare rocks (Papike et al. 1998; Warren and Wasson 1977) share some similarities in mineralogy with NWA 773, but are distinct in key geochemical parameters. Rocks in this group are very diverse, but are generally characterized by feldspar with lower An-contents, mafic silicates with higher $\text{Mg}/(\text{Mg} + \text{Fe})$, and higher mafic silicate:plagioclase feldspar ratios than rocks of the ferroan anorthosite suite (Warren and Wasson 1977). James and Flohr (1983) divided Mg-rich nonmare rocks into norites dominated by orthopyroxene and plagioclase feldspar, and gabbronorites with significant clinopyroxene. NWA 773 clearly bears a closer resemblance to the gabbronorite subgroup in mineralogy, although baddeleyite, which is associated with the norite subgroup (James and Flohr 1983), is present in NWA 773. Inversion of ion microprobe analyses of plagioclase feldspar and pyroxenes from magnesian suite norites, troctolites, and anorthosites indicate that many of these rocks crystallized from liquids with KREEP-like trace element signatures (Papike et al. 1996; Shervais and McGee 1998). In general, this conforms with similar calculations for NWA 773 by Bridges et al. (2002) and with the whole-rock trace element data reported here (Table 9) and elsewhere (Korotev et al. 2002).

In spite of the similarities, NWA 773 differs from some geochemical trends characteristic of the Mg-suite. Although some of the gabbronorites tabulated by James and Flohr (1983) are characterized by moderate LREE-enrichment, none of them has a Eu-anomaly as deep as that of NWA 773. Furthermore, Warren (1986; also see Shearer and Papike 1999) divided the Mg-suite from ferroan anorthosites based on molar $\text{Na}/(\text{Na} + \text{Ca})$ and $\text{Mg}/(\text{Mg} + \text{Fe})$. Using these parameters, the NWA 773 breccia plots in the ferroan anorthosite field, while the olivine gabbro falls along the boundary of values for the Mg-suite and ferroan anorthosites (Fig. 9). The breccia whole-rock composition results from a variety of clasts and cannot be considered “igneous;” thus, the similarity of breccia and ferroan anorthosite values may simply be coincidental. Nonetheless, if, as we propose, the NWA 773 breccia is dominated by rocks from an olivine-gabbro/gabbro/fayalitic-rock differentiation suite, we would expect the breccia whole-rock composition to reflect an intermediate composition between suite endmembers. If NWA 773 truly belongs with the Mg-suite, we would expect the $\text{Na}/(\text{Na} + \text{Ca})$ and $\text{Mg}/(\text{Mg} + \text{Fe})$ values of the breccia and Mg-suite to be similar. The low $\text{Na}/(\text{Na} + \text{Ca})$ of the breccia (Fig. 9) may reflect the Fe-enrichment “tholeiitic” trend we propose for NWA 773 (see FeO-Enrichment Trend and Contrast with SiO_2 -Enrichment in 15405).

Despite these differences, NWA 773 shares some important similarities with the Mg-suite, and NWA 773

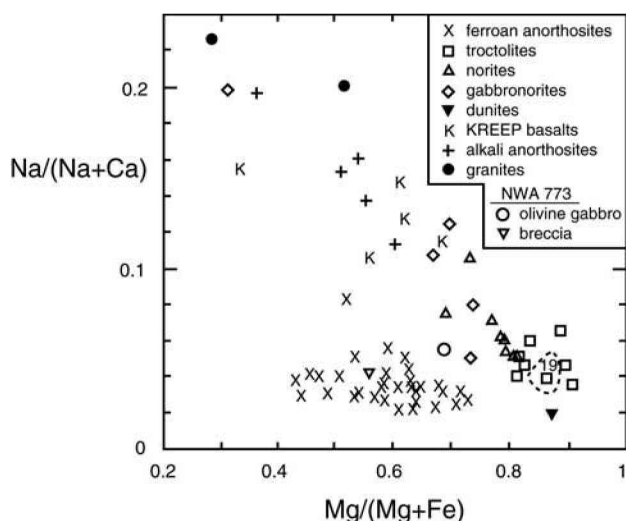


Fig. 9. Discrimination of ferroan anorthosites from Mg-rich rocks based on whole-rock molar $\text{Na}/(\text{Na} + \text{Ca})$ and $\text{Mg}/(\text{Mg} + \text{Fe})$ after Warren (1986) (dashed line at lower right encompasses 19 troctolites). The values for NWA 773 breccia and olivine gabbro are also plotted.

probably shared some elements of petrogenesis with this set of rocks during the magmatic evolution of the moon. Based on mass balance modelling, Warren and Kallemeyn (1993b) propose that up to 30% of the lunar crust is composed of magnesian igneous rocks that intruded into an older ferroan anorthosite crust. The NWA 773 olivine-gabbro/gabbro/fayalitic-rock trend reflects Fe-enrichment during fractionation of a Mg-rich original liquid. This igneous system may have been sited in either a thick lava flow or shallow-level intrusive in the lunar highland crust (James 1980). Possible terrestrial analogues include layered mafic intrusives (Kruger and Marsh 1985; Boudreau and McBirney 1997; McBirney and Nicolas 1997), ophiolitic gabbros (Springer 1980; Pallister and Hopson 1981), sills (Shirley 1987), and ponded lavas (Helz 1987).

CONCLUSIONS

The meteorite Northwest Africa 773 is from the moon. The meteorite consists of two lithologies: a two-pyroxene, cumulate olivine gabbro, and a regolith breccia. The breccia has fragmental textures and includes a variety of materials, but is dominated by gabbroic and fayalite-bearing clasts. The breccia contains large concentrations of solar gases, while the olivine gabbro is solar gas-poor. The $^4\text{He}/^{20}\text{Ne}$ ratio in the breccia fraction is 7.2 ± 0.7 , confirming a lunar origin for NWA 773. The breccia material resided for over 100 Ma in the lunar regolith. The olivine gabbro yields a lunar ejection time of <5.2 Ma and a K-Ar age of 2.75 ± 0.30 Ga. This age is close to that of lunar meteorite Y-793274.

The NWA 773 olivine gabbro lithology and gabbroic and fayalitic lithic fragments in the breccia are from a magmatic

system that evolved by accumulation of olivine, trapping of KREEP-like liquids in intercumulus domains, exsolution of coexisting immiscible silicate liquids, and extreme Fe-enrichment of late-stage liquids. Pyroxene compositional trends from the olivine gabbro lithology show that early accumulation of mafic phases increased $\text{Ti}/(\text{Ti} + \text{Cr})$ of available liquid while $\text{Mg}/(\text{Mg} + \text{Fe})$ remained constant. Eventually, the liquid $\text{Mg}/(\text{Mg} + \text{Fe})$ diminished, resulting in the crystallization of gabbroic rocks with pyroxenes showing a continuous trend of increasing $\text{Ti}/(\text{Ti} + \text{Cr})$ and decreasing $\text{Mg}/(\text{Mg} + \text{Fe})$. The early crystallization of Mg-rich olivine was followed by a hiatus in olivine crystallization; olivine crystallization resumed as the system evolved to very Fe-rich compositions. Two compositionally distinct silicate liquids were present early during crystallization and were trapped as melt inclusions in cumulate olivine. These liquids may have been immiscible. Immiscible liquids may also have been present during late-stage crystallization as the system evolved to very low $\text{Mg}/(\text{Mg} + \text{Fe})$.

From the variety of lithic fragments that appear to be related by magmatic differentiation, we infer that most of the components of NWA 773 are from a complex magmatic body in which the liquid or packets of liquid underwent extreme ranges of Fe-enrichment during crystallization. A likely candidate for this type of magmatic body is a shallow-level layered mafic intrusion, broadly similar to tholeiitic terrestrial intrusions (James 1980) or a ponded lava flow that underwent cumulate differentiation. The presence of agglutinate and a melt spherule with aluminous compositions provides a link to anorthositic rocks and suggests that the olivine-gabbro/gabbro/fayalitic-rock magmatic body was intruded into or extruded on the lunar highland crust.

The LREE-rich trace element signature of NWA 773 is similar to several other mafic lunar meteorites but distinct from the mare basalts sampled during Apollo and Luna missions. The evolution of LREE-rich, mafic rocks in the context of the magmatic evolution of the moon remains to be established.

Acknowledgments—This work was supported by NASA Grants NAG 5-4212 (K. Keil, P. I.) and RTOP 344-31-10-18 (D. W. Mittlefehldt, P. I.), NSF Grant EAR-9815338 (R. N. Clayton, P. I.), and the Swiss National Science Foundation. Much of the manuscript preparation took place at the Tokyo Institute of Technology, where the senior author was supported by a post-doctoral fellowship from the Japan Society for the Promotion of Science. Our assessment of the REE data and comparisons of NWA 773 with lunar and terrestrial rocks benefited from discussions with Masaharu Tanimizu, B. Ray Hawke, and Paul Buchanan. This project owes an obvious debt to Graham Ryder, who proposed a magmatic differentiation trend for igneous clasts in Apollo sample 15405. The manuscript was improved by reviews from D. S. Burnett and R. L. Korotev. This is Hawai'i

Institute of Geophysics and Planetology Publication Number 1238 and School of Ocean and Earth Science and Technology Publication Number 6039.

Editorial Handling—Dr. Urs Krähenbühl

REFERENCES

- Arai T., Takeda H., and Warren P. H. 1996. Four lunar mare meteorites: Crystallization trends of pyroxenes and spinels. *Meteoritics & Planetary Science* 31:877–892.
- Arai T. and Warren P. H. 1999. Lunar meteorite Queen Alexandra Range 94281: Glass compositions and other evidence of launch pairing with Yamato-793274. *Meteoritics & Planetary Science* 34:209–234.
- Arai T., Ishi T., and Otsuki M. 2002. Mineralogical study of a new lunar meteorite Yamato-981031 (abstract #2064). 33rd Lunar and Planetary Science Conference. CD-ROM.
- Bence A. E. and Papike J. J. 1972. Pyroxenes as recorders of lunar basalt petrogenesis: Chemical trends due to crystal-liquid interaction. Proceedings, 3rd Lunar and Planetary Science Conference. pp. 431–469.
- Bence A. E., Papike J. J., and Prewitt C. T. 1970. Apollo 12 clinopyroxenes: Chemical trends. *Earth and Planetary Science Letters* 8:393–399.
- Bence A. E., Papike J. J., and Lindsley D. H. 1971. Crystallization histories of clinopyroxenes in two porphyritic rocks from Oceanus Procellarum. Proceedings, 2nd Lunar and Planetary Science Conference. pp. 559–574.
- Boudreau A. E. and McBirney A. R. 1997. The Skaergaard series Part III: Non-dynamic layering. *Journal of Petrology* 38:1003–1020.
- Bridges J. C., Jeffries T. E., and Grady M. M. 2002. Trace element signatures of trapped KREEP in olivine-rich clasts within lunar meteorite NWA 773. *Meteoritics & Planetary Science* 37:A24.
- Brown G. M. and Vincent E. A. 1963. Pyroxenes from the late stages of fractionation of the Skaergaard intrusion, East Greenland. *Journal of Petrology* 4:175–197.
- Brown R. W. 1977. A sample fusion technique for whole rock analysis with the electron microprobe. *Geochimica et Cosmochimica Acta* 41:435–438.
- Clayton R. N. 1993. Oxygen isotopes in meteorites. *Annual Review of Earth and Planetary Science* 21:115–149.
- Clayton R. N. and Mayeda T. K. 1963. The use of bromine pentafluoride in the extraction of oxygen from oxides and silicates for isotopic analysis. *Geochimica et Cosmochimica Acta* 27:43–52.
- Clayton R. N. and Mayeda T. K. 1975. Genetic relations between the moon and meteorites. Proceedings, 6th Lunar and Planetary Science Conference. pp. 1761–1769.
- Clayton R. N. and Mayeda T. K. 1983. Oxygen isotopes in eucrites, shergottites, nakhlites, and chassignites. *Earth and Planetary Science Letters* 62:1–6.
- Clayton R. N. and Mayeda T. K. 1996. Oxygen isotope studies of achondrites. *Geochimica et Cosmochimica Acta* 60:1999–2017.
- Danyushevsky L. V., McNeill A. W., and Sobolev A. V. 2002. Experimental and petrologic studies of melt inclusions in phenocrysts from mantle-derived magmas: An overview of techniques, advantages, and complications. *Chemical Geology* 183:5–24.
- Delaney J. S. 1989. Lunar basalt breccia identified among Antarctic meteorites. *Nature* 342:889–890.
- Delano J. W. 1986. Pristine lunar glasses: Criteria, data, and implications. Proceedings, 16th Lunar and Planetary Science Conference. pp. D201–D213.
- Dickinson T., Taylor G. J., Keil K., Schmitt R. A., Hughes S. S., and Smith M. R. 1985. Apollo 14 aluminous mare basalts and their possible relationship to KREEP. Proceedings, 15th Lunar and Planetary Science Conference. pp. C365–C374.
- Donaldson C. H. 1976. An experimental investigation of olivine morphology. *Contributions to Mineralogy and Petrology* 57:187–213.
- Eberhardt P., Geiss J., Graf H., Grögler N., Krähenbühl U., Schwaller H., Schwarzmüller J., and Stettler A. 1970. Trapped solar wind noble gases, exposure age, and K/Ar-age in Apollo 11 lunar fine material. Proceedings, 1st Lunar and Planetary Science Conference. pp. 1037–1070.
- Eugster O. and Lorenzetti S. 2001. Exposure history of some differentiated and lunar meteorites. *Meteoritics & Planetary Science* 36:A54–A55.
- Eugster O. and Michel T. 1995. Common asteroid break-up events of eucrites, diogenites and howardites and cosmic-ray exposure production rates for noble gases in achondrites. *Geochimica et Cosmochimica Acta* 59:177–199.
- Eugster O., Michel T. and Niedermann S. 1992. Solar wind and cosmic-ray exposure history of lunar meteorite Yamato-793274. *Proceedings of the NIPR Symposium on Antarctic Meteorites* 5: 21–33.
- Eugster O., Michel T., Niedermann S., Wang D., and Yi W. 1993. The record of cosmogenic, radiogenic, fissionogenic, and trapped noble gases in recently recovered Chinese and other chondrites. *Geochimica et Cosmochimica Acta* 57:1115–1142.
- Fagan T. J., Taylor G. J., Keil K., Bunch T. E., Wittke J. H., Korotev R. L., Jolliff B. L., Gillis J. J., Haskin L. A., Jarosewich E. J., Clayton R. N., Mayeda T. K., Fernandes V. A., Burgess R., Turner G., Eugster O., and Lorenzetti S. 2002. Northwest Africa 032: Product of lunar volcanism. *Meteoritics & Planetary Science* 37:371–394.
- Govindaraju K. 1994. 1994 compilation of working values and sample descriptions for 383 geostandards. *Geostandards Newsletter* 18. 158 p.
- Head J. W. III. and Wilson L. 1992. Lunar mare volcanism: Stratigraphy, eruption conditions, and the evolution of secondary crusts. *Geochimica et Cosmochimica Acta* 56:2155–2175.
- Helz R. T. 1987. Differentiation behavior of Kilauea Iki lava lake, Kilauea volcano, Hawaii: An overview of past and current work. In *Magmatic processes: Physicochemical principles*, edited by Mysen B. O. University Park: The Geochemical Society. pp. 241–258.
- Hess P. C. and Parmentier E. M. 1995. A model of the thermal and chemical evolution of the moon's interior: Implications for the onset of mare volcanism. *Earth and Planetary Science Letters* 134:501–514.
- Hicks T. L., Fagan T. J., and Keil K. 2000. Metamorphic sequence of unequilibrated EH chondrites using modal olivine and silica abundance (abstract #1491). 31st Lunar and Planetary Science Conference. CD-ROM.
- Hicks T. L., Taylor G. J., Fagan T. J., Krot A. N., and Keil K. 2002. Automated mapping of meteorite thin sections using image processing software (abstract #1055). 33rd Lunar and Planetary Science Conference. CD-ROM.
- Hohenberg C. M., Davis P. K., Kaiser W. A., Lewis R. S., and Reynolds J. H. 1970. Trapped and cosmogenic rare gases from stepwise heating of Apollo 11 samples. Proceedings, 1st Lunar and Planetary Science Conference. pp. 1283–1309.
- James O. B. 1980. Rocks of the early lunar crust. Proceedings, 11th Lunar and Planetary Science Conference. pp. 365–393.
- James O. B. and Flohr M. K. 1983. Subdivision of the Mg-suite noritic rocks into Mg-gabbro-norites and Mg-norites.

- Proceedings, 13th Lunar and Planetary Science Conference. pp. A603–A614.
- Jolliff B. L., Korotev R. L. and Rockow K. M. 1998. Geochemistry and petrology of lunar meteorite Queen Alexandra Range 94281, a mixed mare and highland regolith breccia, with special emphasis on very-low-titanium mafic components. *Meteoritics & Planetary Science* 33:581–601.
- Jolliff B. L., Floss C., McCallum I. S., and Schwartz J. M. 1999. Geochemistry, petrology, and cooling history of 14161,7373: A plutonic lunar sample with textural evidence of granitic-fraction separation by silicate-liquid immiscibility. *American Mineralogist* 84:821–837.
- Jolliff B. L., Gillis J. J., Haskin L. A., Korotev R. L., and Wiczorek M. A. 2000. Major lunar crustal terranes: Surface expressions and crust-mantle origins. *Journal of Geophysical Research* 105: 4197–4216.
- Koeberl C., Kurat G., and Brandstätter F. 1993. Gabbroic lunar mare meteorites Asuka-881757 (Asuka-31) and Yamato-793169: Geochemical and mineralogical study. *Proceedings of the NIPR Symposium on Antarctic Meteorites* 6:14–34.
- Korotev R. L., Jolliff B. L., and Haskin L. A. 2000. The concentration of oxygen (and silicon) in lunar materials (abstract #1210). 31st Lunar and Planetary Science Conference. CD-ROM.
- Korotev R. L., Zeigler R. A., Jolliff B. L., and Haskin L. A. 2002. Northwest Africa 773—An unusual rock from the lunar maria. *Meteoritics & Planetary Science* 37:A81.
- Kruger F. J. and Marsh J. S. 1985. The mineralogy, petrology, and origin of the Merensky cyclic unit in the western Bushveld Complex. *Economic Geology* 80:958–974.
- Lawrence D. H., Feldman W. C., Barraclough B. L., Binder A. B., Elphic R. C., Maurice S., Miller M. C., and Prettyman T. H. 2000. Thorium abundances on the lunar surface. *Journal of Geophysical Research* 105:20307–20331.
- Lindsley D. H. 1983. Pyroxene thermometry. *American Mineralogist* 68:477–493.
- Lindsley D. H. and Munoz J. L. 1969. Subsolidus relations along the join hedenbergite-ferrosilite. *American Journal of Science* 267-A:295–327.
- Longhi J. and Bertka C. M. 1996. Graphical analysis of pigeonite-augite liquidus equilibria. *American Mineralogist* 81:685–695.
- McBirney A. R. 1993. *Igneous petrology*. Boston: Jones and Bartlett. 508 p.
- McBirney A. R. and Hunter R. H. 1995. The cumulate paradigm reconsidered. *Journal of Geology* 103:114–122.
- McBirney A. R. and Nicolas A. 1997. The Skaergaard layered series Part II: Magmatic flow and dynamic layering. *Journal of Petrology* 38:569–580.
- McBirney A. R. and Noyes R. M. 1979. Crystallization and layering of the Skaergaard intrusion. *Journal of Petrology* 20:487–554.
- Mittlefehldt D. W. 1994. The genesis of diogenites and HED parent body petrogenesis. *Geochimica et Cosmochimica Acta* 58:1537–1552.
- Naney M. T., Crowl D. M., and Papike J. J. 1976. The Apollo 16 drill core: Statistical analysis of glass chemistry and the characterization of a high alumina-silica poor (HASP) glass. Proceedings, 7th Lunar and Planetary Science Conference. pp. 155–184.
- Neal C. R. and Taylor L. A. 1992. Petrogenesis of mare basalts: A record of lunar volcanism. *Geochimica et Cosmochimica Acta* 56:2177–2211.
- Neal C. R., Hacker M. D., Snyder G. A., Taylor L. A., Liu Y. G., and Schmitt R. A. 1994. Basalt generation at the Apollo 12 site, Part 2: Source heterogeneity, multiple melts, and crustal contamination. *Meteoritics* 29:349–361.
- Norman M. D. and Mittlefehldt D. W. 2002. Impact processing of chondritic planetesimals: Siderophile and volatile element fractionation in the Chico L chondrite. *Meteoritics & Planetary Science* 37:329–344.
- Norman M. D., Griffin W. L., Pearson N. J., Garcia M. O., and O'Reilly S. Y. 1998. Quantitative analysis of trace element abundances in glasses and minerals: A comparison of laser ablation ICPMS, solution ICPMS, proton microprobe, and electron microprobe data. *Journal of Analytical Atomic Spectroscopy* 13:477–482.
- Norman M. D., Garcia M. O., Kamenetsky V. S., and Nielsen R. L. 2002. Olivine-hosted melt inclusions in Hawaiian picrites: Equilibration, melting, and plume source characteristics. *Chemical Geology* 183:143–168.
- Pallister J. S. and Hopson C. A. 1981. Samail ophiolite plutonic suite: Field relations, phase variation, cryptic variation and layering, and a model of a spreading ridge magma chamber. *Journal of Geophysical Research* 86:2593–2644.
- Papike J. J. 1998. Comparative planetary mineralogy: Chemistry of melt-derived pyroxene, feldspar, and olivine. In *Planetary materials*, edited by Papike J. J. Washington D.C.: Mineralogical Society of America. pp. 7–1–7–11.
- Papike J. J., Fowler W. G., Shearer C. K., and Layne G. D. 1996. Ion microprobe investigation of plagioclase and orthopyroxene from lunar Mg-suite norites: Implications for calculating parental melt REE concentrations and for assessing postcrystallization REE redistribution. *Geochimica et Cosmochimica Acta* 60:3967–3978.
- Papike J. J., Ryder G., and Shearer C. K. 1998. Lunar samples. In *Planetary materials*, edited by Papike J. J. Washington D.C.: Mineralogical Society of America. pp. 5–1–5–234.
- Polnau E. and Eugster O. 1998. Cosmic-ray produced, radiogenic, and solar noble gases in lunar meteorites Queen Alexandra Range 94269 and 94281. *Meteoritics & Planetary Science* 33: 313–319.
- Roedder E. 1978. Silicate liquid immiscibility in magmas and in the system $K_2O-FeO-Al_2O_3-SiO_2$: An example of serendipity. *Geochimica et Cosmochimica Acta* 42:1597–1617.
- Roedder E. and Weiblen P. W. 1971. Petrology of silicate melt inclusions, Apollo 11 and 12 and terrestrial equivalents. Proceedings, 2nd Lunar and Planetary Science Conference. pp. 507–528.
- Rutherford M. J., Hess P. C., and Daniel G. H. 1974. Experimental liquid line of descent and liquid immiscibility for basalt 70017. Proceedings, 5th Lunar and Planetary Science Conference. pp. 569–583.
- Ryder G. 1976. Lunar sample 15405: Remnant of a KREEP basalt-granite differentiated pluton. *Earth and Planetary Science Letters* 29:255–268.
- Ryder G. and Schuraytz B. C. 2001. Chemical variation of the large Apollo 15 olivine-normative mare basalt rock samples. *Journal of Geophysical Research* 106:1435–1451.
- Ryerson F. J. and Hess P. C. 1978. Implications of liquid-liquid distribution coefficients to mineral-liquid partitioning. *Geochimica et Cosmochimica Acta* 42:921–932.
- Sack R. O. and Ghiorso M. S. 1994. Thermodynamics of multicomponent pyroxenes: II. Phase relations in the quadrilateral. *Contributions to Mineralogy and Petrology* 116: 287–300.
- Schmitt H. H. 1991. Evolution of the moon: Apollo model. *American Mineralogist* 76:773–784.
- Shearer C. K. and Papike J. J. 1999. Magmatic evolution of the moon. *American Mineralogist* 84:1469–1494.
- Shearer C. K., Wiedenbeck M., Spilde M. N., and Papike J. J. 1997. Minor and trace element partitioning between immiscible high-Fe basalts and high-Si rhyolites: An example from melt

- inclusions in mare basalts (abstract #1236). 27th Lunar and Planetary Science Conference. CD-ROM.
- Shervais J. W. and McGee J. J. 1998. Ion and electron microprobe study of troctolites, norite, and anorthosites from Apollo 14: Evidence for urKREEP assimilation during petrogenesis of Apollo 14 Mg-suite rocks. *Geochimica et Cosmochimica Acta* 62:3009–3023.
- Shirley D. N. 1987. Differentiation and compaction in the Palisades sill, New Jersey. *Journal of Petrology* 28:835–865.
- Simon S. B., Papike J. J., Hörz F., and See T. H. 1985. An experimental investigation of agglutinate melting mechanisms: Shocked mixtures of sodium and potassium feldspars. Proceedings, 16th Lunar and Planetary Science Conference. pp. D103–D115.
- Snyder G. A., Taylor L. A., and Patchen A. 1999a. Lunar meteorite EET 96008, Part I. Petrology and mineral chemistry: Evidence of large-scale, late-stage fractionation (abstract #1499). 30th Lunar and Planetary Science Conference. CD-ROM.
- Snyder G. A., Neal C. R., Ruzicka A. M., and Taylor L. A. 1999b. Lunar meteorite EET 96008, Part II: Whole-rock trace-element and PGE chemistry, and pairing with EET 87521 (abstract #1705). 30th Lunar and Planetary Science Conference. CD-ROM.
- Springer R. K. 1980. Geology of the Pine Hill intrusive complex, a layered gabbroic body in the western Sierra Nevada foothills, California: Summary. *Geological Society of America Bulletin* 91: 381–385.
- Steele A. M., Colson R. O., Korotev R. L., and Haskin L. A. 1992. Apollo 15 green glass: Compositional distribution and petrogenesis. *Geochimica et Cosmochimica Acta* 56:4075–4090.
- Tanimizu M. and Tanaka T. 2002. Coupled Ce-Nd isotope systematics and REE differentiation of the moon. *Geochimica et Cosmochimica Acta* 66:4007–4014.
- Taylor G. J., Warner R. D., Keil K., Ma M. S., and Schmitt R. A. 1980. Silicate liquid immiscibility, evolved lunar rocks and the formation of KREEP. In *Proceedings of the Conference on the lunar highlands crust*, edited by Papike J. J. and Merrill R. B. New York: Pergamon Press. pp. 339–352.
- Taylor L. A., Nazarov M. A., Demidova S. I., and Patchen A. 2001. Dhofar 287: A new lunar mare basalt from Oman. *Meteoritics & Planetary Science* 36:A204.
- Thompson J. B. Jr. 1982. Composition space: An algebraic and geometric approach. In *Characterization of metamorphism through mineral equilibria*, edited by Ferry J. M. Washington D.C.: Mineralogical Society of America. *Reviews in Mineralogy* 10:1–31.
- Warren P. H. 1985. The lunar magma ocean concept. *Annual Review of Earth and Planetary Science* 13:201–240.
- Warren P. H. 1986. Anorthosite assimilation and the origin of the Mg/Fe-related bimodality of pristine Moon rocks: Support for the magmasphere hypothesis. Proceedings, 16th Lunar and Planetary Science Conference. pp. D331–D343.
- Warren P. H. 1993. A concise compilation of petrologic information on possibly pristine nonmare Moon rocks. *American Mineralogist* 78:360–376.
- Warren P. H. and Kallemeyn G. W. 1989. Elephant Moraine 87521: The first lunar meteorite composed of predominantly mare material. *Geochimica et Cosmochimica Acta* 53:3323–3300.
- Warren P. H. and Kallemeyn G. W. 1991b. The MacAlpine Hills lunar meteorite, and implications of the lunar meteorites collectively for the composition and origin of the Moon. *Geochimica et Cosmochimica Acta* 55:3123–3138.
- Warren P. H. and Kallemeyn G. W. 1991a. Geochemical investigation of five lunar meteorites: Implications for the composition, origin, and evolution of the lunar crust. *Proceedings of the NIPR Symposium on Antarctic Meteorites* 4:91–117.
- Warren P. H. and Kallemeyn G. W. 1993a. Geochemical investigation of two lunar meteorites: Yamato-793169 and Asuka-881757. *Proceedings of the NIPR Symposium on Antarctic Meteorites* 6:35–57.
- Warren P. H. and Kallemeyn G. W. 1993b. The ferroan-anorthositic suit, the extent of lunar melting, and the bulk composition of the moon. *Journal of Geophysical Research* 98:5445–5455.
- Warren P. H. and Wasson J. T. 1977. Pristine nonmare rocks and the nature of the lunar crust. Proceedings, 8th Lunar and Planetary Science Conference 8:2215–2235.
- Yagi K. and Takeshita H. 1987. Impact of hornblende crystallization for the genesis of calc-alkalic andesites. In *Magmatic processes: Physicochemical principles*, edited by Mysen B. O. University Park: The Geochemical Society. pp. 183–190.
- Yanai K. and Kojima H. 1991. Varieties of lunar meteorites recovered from Antarctica. *Proceedings of the NIPR Symposium on Antarctic Meteorites* 4:70–90.
-

APPENDIX

Table A1. Results ($\mu\text{g/g}$) of ICP-MS analyses from NWA 773.

	"Clast"			Breccia		
	Run 1	Run 2	Mean	Run 1	Run 2	Mean
Li	7.5	7.6	7.6	9.5	9.7	9.6
Sc	26.6	26.9	26.8	39.7	38.8	39.3
Ti	2852	2889	2870	5265	5080	5170
V	81	83	82	134	131	132
Cr	2297	2306	2300	2709	2613	2660
Co	95	97	96	65	64	65
Ni	210	217	214	121	124	122
Cu	6	7	7	12	12	12
Zn	11	11	11	8	9	9
Ga	3.1	3.2	3.2	4.1	4.1	4.1
Rb	1.8	1.9	1.8	3.4	3.4	3.4
Sr	39.9	40.8	40.3	60.1	61.2	60.7
Y	30.8	31.0	30.9	54.9	56.4	55.6
Zr	164	171	167	242	250	246
Nb	8.9	9.3	9.1	13.8	14.2	14.0
Mo	0.25	0.32	0.28	0.26	0.32	0.29
Cd	0.045	0.045	0.045	0.052	0.054	0.053
Sn	0.6	0.6	0.6	22.6	19.0	20.8
Sb	0.009	0.008	0.009	0.011	0.008	0.010
Cs	0.063	0.061	0.062	0.150	0.150	0.150
Ba	151	147	149	161	159	160
La	8.2	7.9	8.0	14.1	13.8	14.0
Ce	21.5	20.7	21.1	37.1	36.4	36.8
Pr	2.90	2.76	2.83	5.01	4.89	4.95
Nd	13.6	13.1	13.3	23.7	23.0	23.4
Sm	3.95	3.78	3.87	6.96	6.77	6.86
Eu	0.38	0.38	0.38	0.62	0.60	0.61
Gd	4.57	4.44	4.50	8.16	7.96	8.06
Dy	5.15	5.01	5.08	9.58	9.47	9.53
Ho	1.12	1.08	1.10	2.10	2.05	2.07
Er	2.99	2.86	2.93	5.68	5.53	5.60
Yb	2.90	2.86	2.88	5.67	5.65	5.66
Lu	0.43	0.41	0.42	0.83	0.82	0.83
Hf	3.37	3.34	3.36	5.44	5.35	5.40
Ta	0.37	0.38	0.37	0.63	0.63	0.63
Th	1.30	1.26	1.28	2.31	2.30	2.31
U	0.32	0.31	0.32	0.61	0.60	0.61